Molecular Physics, Vol. 00, No. 00, 20 January 2006, 1–23

Quantum monodromy, its generalizations and molecular manifestations

D. A. Sadovskií and B. I. Zhilinskií*

Université du Littoral, UMR 8101 du CNRS, 59140 Dunkerque, France

(*January 2006*)

Quantum monodromy is a nontrivial qualitative characteristics of certain nonregular lattices formed by the joint eigenvalue spectrum of mutually commuting operators. The latter are typically the hamiltonian (energy) and the momentum operator(s) which label the eigenstates of the system. We give a brief review of known quantum systems with monodromy, which include such fundamental systems as the hydrogen atom in external fields, Fermi resonant vibrations of the CO_2 molecule, and nonrigid triatomic molecules. We emphasize the correspondence between the classical hamiltonian monodromy and its quantum analog and discuss possible generalizations of this characteristics in classical integrable hamiltonian dynamical systems and their quantum counterparts.

1 Introduction

Classical hamiltonian monodromy was introduced by Duistermaat in 1980 [1] to describe the simplest possible obstruction to the existence of global action-angle variables [2] in completely integrable classical hamiltonian dynamical systems. At the time, it was considered as just an interesting exercise in differential geometry with no important physical consequences in concrete dynamical systems. It took almost a decade for the quantum analog of this concept to be formulated [3]. Notice that the absence of global action-angle variables translates for the quantum system into the absence of global quantum numbers. As a consequence, the energy of all states of such system cannot be represented by a single smooth function (often called 'term' in spectroscopy) of the quantum numbers.

First concrete examples of fundamental dynamical systems with monodromy, notably the spherical pendulum and the Lagrange top, were studied in great detail by Cushman [4,5]. Cushman presented these results to theoretical physicists and chemists at a number of conferences and insisted on the possible importance and relevance of monodromy in many concrete physical systems. It is largely due to his effort and intuition, that analysis of monodromy has become an important direction in modern molecular and atomic physics.

Nowadays, the presence of monodromy and its importance for qualitative understanding of classical and quantum systems has been demonstrated eloquently on a considerable number of concrete atomic and molecular examples, such as the hydrogen atom in orthogonal electric and magnetic fields [6–8], coupling of angular momenta in the presence of axial or rotational symmetry [9,10], vibrations of quasilinear molecules near the barrier to linearity [11,12], molecular hydrogen ion and associated three particle systems [13,14], triatomic nonrigid molecules with diatomic rigid core [15,16], vibrations of linear triatomic molecules with Fermi resonance [17–19], rotation of dipolar molecules in electric field [20,21].

In its turn, this rapid advancement of physical applications stimulated further analysis and more sophisticated mathematical constructions [5,22]. At present, the work on the mathematical foundations of monodromy and associated qualitative phenomena involves a considerable collective effort of mathematicians, physicists, and theoretical chemists. Such collaboration requires a common framework of mathematical

*Corresponding author. Email: zhilin@univ-littoral.fr

Molecular Physics
ISSN 0026-8976 print/ ISSN 1362-3028 online
http://www.tandf.co.uk/journals
DOI: 10.1080/002689700xxxxxxxxxxxx

tools, formal concepts, and terminology. However, the language used in different communities working on essentially the same class of phenomenon remains quite different. This situation is, perhaps, unavoidable in a young and dynamic domain of research, where the frontiers are not yet well established and where review articles and monographs lag well behind the latest work.

In the contemporary research work on quantum monodromy, the above differences are particularly visible. Quantum monodromy appeals in most direct ways to a broad non-specialist community of molecular physicists, spectroscopists, and theoretical chemists, who study the energy level spectra of concrete molecular systems. The abstract theoretical formulation of quantum monodromy was developed by San [23] following the initial idea in [3]. A closely related interpretation of quantum monodromy in terms of lattice defects (see [24–26]) was proposed at the same time and has quickly become the tool of choice in applications [9]. We will give several concrete illustrations of this approach.

In his recent survey of applications of quantum monodromy [27], Child describes several important molecular systems with monodromy. We attempt to complement this review with a brief discussion of more recent developments, notably a number of generalizations, which have not yet found their way in the atomic and molecular literature. We focus on the qualitative aspects and do not enter into details of the rigorous mathematical formalism. Instead, we introduce on a somewhat intuitive level a number of basic concepts, such as the energy-momentum map EM or the toric fibration, and then use them to describe and characterize the lattices of points formed by the eigenvalues of several mutually commuting observables.

2 Basic concepts

In this paper, we consider a number of model quantum systems with N degrees of freedom, where N is usually 2 or in some cases 3. In concrete applications such models correspond to a subsystem of a complete molecular or atomic system which is described by an effective quantum Hamiltonian. For simplicity, we restrict ourselves to Hamiltonians written in terms of Cartesian coordinates q_k and conjugate momenta p_k with $k = 1, \ldots, N$. (Specifically, one can think of an effective vibrational Hamiltonian describing several coupled small vibrations near an equilibrium.) In this situation, going from the quantum system to its classical limit simply means replacing quantum operators $\hat{q}_i$ and $\hat{p}_i$ by their classical analogs. In order to work with quantum monodromy we should first recall several important concepts related primarily to the classical limit system.

2.1 *Integrability, symmetries, normalization*

Classical monodromy is a property of certain completely integrable classical systems. Such systems have N functionally independent functions $F_1, \ldots, F_N$, where as before N is the number of degrees of freedom, which are mutually in involution, i.e., all Poisson brackets $\{F_k, F_l\}$ with $k \neq l$ are zero. We will, therefore, consider quantum systems with completely integrable classical counterparts. Such quantum systems have N linearly independent mutually commuting observables $\hat{F}_1, \ldots, \hat{F}_N$.

The integrals of motion $F_1, \ldots, F_N$ (or first integrals) may be related to continuous (or Lie) symmetries of the system. Such symmetries can be strict or approximate; they can also be spatial, spatial-temporal, and dynamical. Spatial symmetries have dual action: they do not mix coordinates and momenta, and their action on the momenta replicates that on the coordinates. For example we will consider an axial symmetry which acts as an S^1 rotation of the q-space. Dynamical symmetries are of a more general kind.

Thus we consider the *polyad symmetries* which are certain S^1 rotations of the (q, p)-space, and related *polyad integrals* and corresponding *polyad quantum numbers*. The polyad symmetry is typically approximate and is introduced on the basis of physical assumptions. It becomes an exact symmetry for the system whose Hamiltonian is *normalized* and *truncated* at some order. At the same time, the polyad integral and the corresponding quantum number become exact. In classical mechanics, normalization is usually performed using Lie transform techniques (or older variants of classical perturbation theory), the direct quantum analog of such technique is known as Van Vleck transformation. Note that for brevity we often speak of normalized system and normalized or polyad Hamiltonian. In physical applications, such

Hamiltonians are often called *model* since they rely on a particular polyad assumption, and *effective* since normalization often averages out some degrees of freedom thus reducing the dimension of the problem.

2.2 *Energy-momentum mapping, its image and fibers*

Description of Hamiltonian monodromy relies on the fundamental concept of *energy-momentum map* EM or generalized momentum map [5, 28, 29] which can be introduced for any completely integrable classical system. EM sends (a domain of) the initial $2N$-dimensional phase space $\mathbb{R}^{2N}_{q,p}$ to (a domain of) the N-dimensional space of the values $f = (f_1, \ldots, f_N)$ of N integrals of motion $F_1, \ldots, F_N$. The name 'energy-momentum' originated in the situation where some of the first integrals define periodic flows on *all* regular tori. In other words, they are generators of global $\mathbb{S}^1$ symmetry actions on $\mathbb{R}^{2N}_{q,p}$, such as, for example, simultaneous rotation of the q and the p-space about an axis. Such first integrals are called *momenta*. If all $F_1, \ldots, F_N$ are of this kind, they define a momentum map [30]. However, in a more common situation, some F_k, and in particular the Hamiltonian of the system, define nonperiodic flows.

Generically, the subspace of $\mathbb{R}^{2N}_{q,p}$ associated with a given value f_k of an integral of motion F_k, or the constant f_k*-level set* of F_k, is of dimension $N-1$. A common f-level set of N first integrals can be represented in $\mathbb{R}^{2N}_{q,p}$ as an intersection of N subspaces each of dimension $N-1$. Such common level set is a *dynamically invariant subspace* of $\mathbb{R}^{2N}_{q,p}$. It includes all points of $\mathbb{R}^{2N}_{q,p}$ at which the value of EM is f, and can be denoted as the inverse image $\mathrm{EM}^{-1}(f)$ of f. Once started on $\mathrm{EM}^{-1}(f)$, a trajectory of any system with first integrals $F_1, \ldots, F_N$ will remain there.

It can be seen that $\mathrm{EM}^{-1}(f)$ is, generically, of dimension N. Furthermore, since we will only consider bound states, $\mathrm{EM}^{-1}(f)$ is compact. Applying the Liouville-Arnol'd theorem [5, 31] for all regular values[1] f of EM, we conclude that connected components of $\mathrm{EM}^{-1}(f)$ are N-dimensional tori $\mathbb{T}^N_f$, often called invariant or Liouville tori. This means that EM defines a *toric fibration*, whose base space is the image of EM and whose generic fibers[2] are $\mathbb{T}^N$.

Critical fibers[2] of EM can have dimension lower than N, for example an equilibrium point, a periodic orbit (relative equilibrium). Any point on such lower-dimensional fibers is a critical point of EM. Alternatively, critical fibers can be singular varieties of dimension N. All of them can include both critical and regular

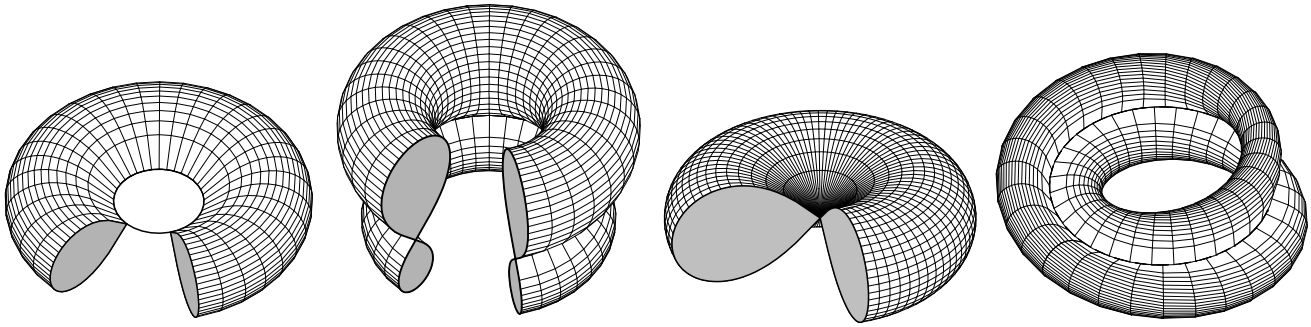

Figure 1. Two-dimensional singular fibers in the case of integrable Hamiltonian systems with two degrees of freedom (left to right): singular torus, bitorus, pinched and curled tori. Only the singular torus is topologically equivalent (but not diffeomorphic) to a 2-torus.

points of EM. To have an example, see fig. 1 which presents singular fibers for $N = 2$ which we will encounter later. For example, bitorus appears in LiNC, HNC models (see sec. 6.1), pinched torus appears in spherical pendulum, "champagne bottle", or $1 : (-1)$ resonance oscillator models (see sec. 3), curled torus is a characteristic singularity for models with fractional monodromy (see sec. 5). Furthermore, a complete preimage $\mathrm{EM}^{-1}(c)$ of a critical value c can be a union[2] of any number of different disconnected critical fibers and regular N-tori.

[1]Recall that the point ξ of the initial phase space $\mathbb{R}^{2N}_{q,p}$ is a *regular point* of EM, and the corresponding value $f = \mathrm{EM}(\xi)$ is a *regular value* if the differentials $(dF_1, dF_2, \ldots, dF_N)$ are linearly independent at ξ. Alternatively, if $(dF_1, dF_2, \ldots, dF_N)$ are linearly dependent at some point ξ_c, the latter is a *critical point* of EM, and the corresponding value $f_c = \mathrm{EM}(\xi_c)$ is a *critical value*.

[2]Notice that by fiber over f we imply a connected component of $\mathrm{EM}^{-1}(f)$, the latter can therefore be a union of fibers.

The image $\mathcal{R}$ of the EM map is a N-dimensional domain in $\mathbb{R}^N$ which includes necessarily both regular and critical values. Regular values form an open N-dimensional subspace $\mathcal{R}_{\rm reg}$, which can be a disjoint union of one or several open connected components. Critical values can form critical subspaces of different dimensions and can be characterized additionally by their *codimension*.[3] In particular, critical values form the boundary of $\mathcal{R}$. Thus in the case $N = 2$ (i.e., for completely integrable Hamiltonian systems with two degrees of freedom) the sets $\mathcal{R}$ and $\mathcal{R}_{\rm reg}$ are of dimension two. Critical values can form subspaces of codimension 1 or 2, which are lines or isolated points in $\mathcal{R}$, respectively. Examples of the images $\mathcal{R}$ for $N = 2$ which are relevant to our discussion are presented schematically in fig. 2.

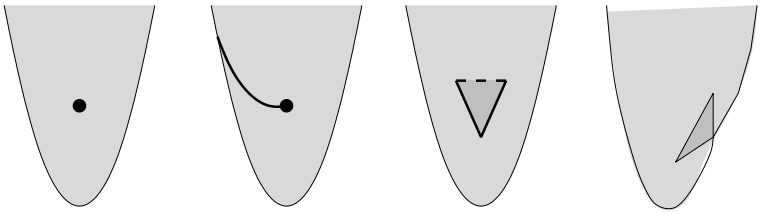

Figure 2. Typical images $\mathcal{R}$ of the EM map for completely integrable Hamiltonian systems with two degrees of freedom in the case of integer monodromy, fractional monodromy, nonlocal monodromy, and bidromy (left to right). Critical values are shown by solid lines and dot (codimension 1 and 2); light shaded area represents the set of regular values $\mathcal{R}_{\rm reg}$ which lift to a single 2-torus, values in the dark shaded area lift to two 2-tori.

2.3 *Generalized action-angle variables*

Generalized action-angle variables [2] are defined on regular N-tori. Besides serving as coordinates on the tori, they give direct relation to quantum mechanics by means of the EBK quantization. For a given regular fiber $\mathbb{T}^N_f$, generalized actions $I_1, \ldots, I_N$ are constructed as Hamiltonian functions $I_1(q,p), \ldots, I_N(q,p)$ which define N *periodic* hamiltonian flows on $\mathbb{T}^N_f$ as well as on its immediate neighbours. Since each I_k defines a circle action (a rotation) it is a *momentum* (cf sec. 2.2); the conjugate angle φ_k is the natural coordinate along the $\mathbb{S}^1$ orbit of this action. Notice that geometrically the system of periodic trajectories associated with actions $I_1, \ldots, I_N$ generates *cycle bases* of the fundamental groups π_1 or homology groups H_1 of all regular tori $\mathbb{T}^N$ in the domain of the definition of $I_1, \ldots, I_N$. In this domain the cycle bases are related smoothly among themselves, thus defining isomorphisms between all tori involved. Locally, i.e., in a sufficiently small simply connected open neighborhood of $\mathbb{T}^N_f$ which contains only regular fibers, constructing $I_1, \ldots, I_N$ is always possible by the Liouville–Arnol'd theorem [5, 31]. This means that our toric fibrations are locally regular.

Since actions $I_1, \ldots, I_N$ are constants for any given invariant torus, they are built normally from the initial set of first integrals $F_1, \ldots, F_N$. For each I_k this gives its pull-back $I_k : \mathrm{EM}(U) \to \mathbb{R} : f \to I_k(\mathrm{EM}^{-1}(f))$ under EM^{-1}. In other words, we can consider functions $I_1, \ldots, I_N$ on the image of the energy-momentum map. This has the obvious advantage of working in the base of dimension N instead of the total $2N$-dimensional space of the fibration.

Consider now a larger neighborhood U of $\mathbb{T}^N_f$. In the simplest situation, the image $\mathrm{EM}(U(\mathbb{T}^N_f))$ is an open N-ball in $\mathcal{R}_{\rm reg}$ which contains f. (If $\mathrm{EM}(U)$ is the whole $\mathcal{R}_{\rm reg}$ then we attempt to define global actions on the whole $2N$-dimensional domain $\mathrm{EM}^{-1}(\mathcal{R}_{\rm reg})$ in $\mathbb{R}^{2N}_{q,p}$.) If that is the case, defining $I_1, \ldots, I_N$ on the whole of U is possible. In other words the 2-torus bundle over $\mathrm{EM}(U)$ is trivial and we have one global momentum map $U \mapsto \mathbb{R}^N$.

The argument can be well illustrated on the example with $N = 2$. In this case $\mathrm{EM}(U)$ is an open disk of regular values which contains the regular value $f = (0, 0)$ as shown in fig. 3, left. We choose a closed directed contour Γ in $\mathrm{EM}(U)$. All points of Γ are, obviously, regular values. Let f^0 be a starting point on Γ. We define local action-angle variables on and near $\mathbb{T}^2_{f^0} = \mathrm{EM}^{-1}(f^0)$ and then extend them smoothly as we move along Γ. As we come back to $f^1 = f^0$ after making a tour, we should verify whether the action-angle

[3] Codimension equals the difference between the dimension of the space and the dimension of the subspace.

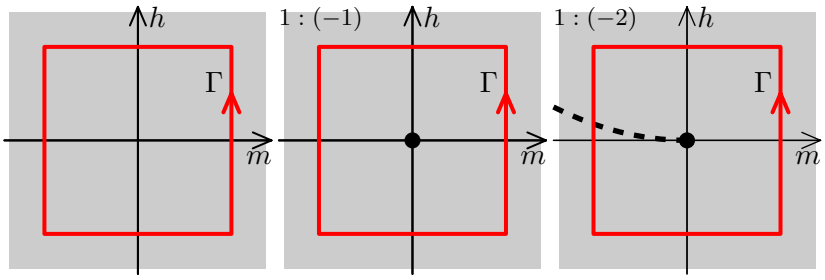

Figure 3. Images of the energy-momentum map EM near the value $0 \in \mathbb{R}^2_{m,h}$ (left to right) for the regular case, and for the 1:(−1), and 1:(−2) nonlinear resonant oscillator systems. Shaded area represents regular values of EM, black dot marks the isolated critical value 0, and bold dotted line shows the line of critical values which correspond to curled tori. The closed contour Γ is used to compute monodromy as explained in sec. 2.4.

coordinates which we obtained in f^1 by this extension are the same as those we began with in f^0. To this end we use the fact that Γ is *contractible* in $\mathrm{EM}(U)$ to a point, i.e., the homotopy class of Γ is 0. We can therefore deform Γ continuously in order to get the whole of Γ inside a sufficiently small open regular neighborhood of $f = (0, 0)$. Then local action-angle coordinates on and near $\mathbb{T}^2_f$ cover the whole $\mathrm{EM}^{-1}(\Gamma)$ and are the same for f^0 and f^1. Since the deformation was continuous this applies to the original Γ and therefore angle-action variables exist globally for all tori whose images lie inside Γ, i.e., basically on the whole U.

General conditions for the existence of global action–angle variables are detailed in [2]. The topological analysis of the image of EM gives indication on whether and in what domains global action–angle variables exist. Thus, if in the above example, $\mathrm{EM}(U)$ is not simply connected, global actions do not exist on U. It is also important to notice that global functions $I_k \circ \mathrm{EM}^{-1}$ with $k = 1, \ldots, N$ are *smooth* real single-valued functions on U. This should not be forgotten when functions like $|F_1|$ are used in order to label the tori and to define the corresponding quantum numbers. In fact, if expressions for $I_1, \ldots, I_N$ use $|F_1|$, we have two different sets of global action-angle coordinates, one for $F_1 \leq 0$ and the other for $F_1 \geq 0$.

2.4 *Hamiltonian monodromy and its generalizations*

Classical Hamiltonian monodromy was introduced in [1] (see also [5]) as the simplest obstruction to the existence of global action–angle variables. Such obstruction is caused by the presence inside the regular value domain $\mathcal{R}_{\mathrm{reg}}$ of isolated subspaces $\mathcal{C}^{N-2}$ of critical values of codimension 2. Indeed, we can attempt to verify if global actions exist using the approach in sec. 2.3. However, we realize immediately that due to the presence of $\mathcal{C}^{N-2}$, there exist nontrivial closed paths Γ which lie entirely in $\mathcal{R}_{\mathrm{reg}}$ but are *not* contractible to a point because they 'encircle' one or several subspaces $\mathcal{C}^{N-2}$.

A concrete example system with $N = 2$ is discussed in sec. 3. In this case, the isolated subspace of codimension 2 is a point which lies inside $\mathcal{R}_{\mathrm{reg}}$, i.e., a single critical value surrounded by regular values. As we can see in fig. 3, centre, a contour Γ, which goes around such point is not contractible. As a consequence, global action-angle variables do not exist on $\mathrm{EM}^{-1}(\Gamma)$ and therefore on $\mathrm{EM}^{-1}(\mathcal{R}_{\mathrm{reg}})$. If we pursue constructing such variables as described in sec. 2.3, we would end up with local action-angles for f^1 which differ from those we had originally for f^0. In other words, we would have two different cycle bases on the same torus $\mathbb{T}^2_{f_0}$. These two bases are related by the *monodromy transformation* which is given by a *monodromy matrix*[1] M in $\mathrm{SL}(2, \mathbb{Z})$. Notice that this matrix is defined with respect to some fixed cycle basis on $\mathbb{T}^2_{f_0}$ (fixed choice of local actions), usually the initial basis in f_0. The choice of this basis is arbitrary, we can redefine it using a similarity transformation with matrix A in $\mathrm{SL}(N, \mathbb{Z})$. It follows that M is defined up to a conjugation AMA^{-1} within the $\mathrm{SL}(N, \mathbb{Z})$ group[1], i.e., M represents a *class* of conjugated elements of $\mathrm{SL}(N, \mathbb{Z})$. The situation here is similar to crystallography. The choice of the basis of crystal lattice is ambigous. Different bases are related among themselves by $SL(3, Z)$ transformation which changes the form of elementary crystallographic cell but leaves its volume constant.

[1]Matrices M in the group $\mathrm{SL}(N, \mathbb{Z})$ are $N \times N$ matrices with integer entries and $\det M = 1$.

It is important to note that monodromy is a very robust characteristics. It does not depend on the choice of the initial and final point $f^0 = f^1$ on the path Γ, neither on the choice of this path itself (within the class of homotopically equivalent paths), nor on sufficiently small modifications of parameters of the system, which do not destroy complete integrability and do not change qualitatively the image of the EM map.

Furthermore, it has been conjectured in [7] and then demonstrated rigorously in [32,33] that monodromy 'survives' the breakdown of exact integrability and the onset of 'weak' chaos as long as most of the KAM tori of the perturbed system remain intact. This result is of great consequence to our applications since practically all real atomic and molecular systems are nonintegrable. On the other hand, our systems are known for a hierarchy of perturbations and for good near integrability and sometimes even separability at different levels of approximation. Such systems are described commonly within the perturbation theory framework, where the full original Hamiltonian is normalized and truncated at a desired order and the truncated normal form provides a reasonable integrable approximation to the dynamics. Notice also that the situation improves considerably when we transfer our results to quantum analogs of our systems which are to a certain extent 'liberated from classical chaos' [34].

Topological character of monodromy and structural stability of this property is elucidated by the fact that the monodromy transformation is determined entirely by the topological type of the singular fiber (the so-called geometric monodromy theorem) [35–37]. From this point of view, even the requirement for the system to be Hamiltonian can be dropped. In the simplest case of $N = 2$, the fiber which causes monodromy is the 'celebrated' singly pinched torus shown in fig. 1, second right. This fiber is the preimage $\mathrm{EM}^{-1}(0)$ of the isolated critical value $0 = (0, 0)$ in fig. 2, left, and fig. 3, centre. In the appropriately chosen cycle basis, the corresponding matrix is $\left(\begin{smallmatrix} 1 & 1 \\ 0 & 1 \end{smallmatrix}\right)$. As shown in [35, 38], a similar fiber but with 2 pinches (see example in [7]) results in matrix $\left(\begin{smallmatrix} 1 & 2 \\ 0 & 1 \end{smallmatrix}\right)$. Under the variation of the cycle basis the form of the monodromy matrix changes. If $A = \left(\begin{smallmatrix} a & b \\ c & d \end{smallmatrix}\right)$ is a $SL(2, Z)$ matrix with integer entries a, b, c, d and with $ad - bc = 1$, which describes the modification of the cycle basis, the corresponding explicit modification of the elementary monodromy matrix $\left(\begin{smallmatrix} 1 & 1 \\ 0 & 1 \end{smallmatrix}\right)$ can be written in the form

$$\begin{pmatrix} a & b \\ c & d \end{pmatrix} \begin{pmatrix} 1 & 1 \\ 0 & 1 \end{pmatrix} \begin{pmatrix} d & -b \\ -c & a \end{pmatrix} = \begin{pmatrix} 1 - ac & a^2 \\ -c^2 & 1 + ac \end{pmatrix}.$$

Remaining in the lowest dimensional situation of $N = 2$, most radical generalizations of classical Hamiltonian monodromy can be obtained by extending the class of admissible paths from paths which include only regular values of the EM map to more general paths which can cross codimension-1 subsets $\mathcal{C}^1$ of critical values of the EM map, i.e., paths crossing (transversely) lines of critical values. (Notice that such intersections occur generically in $\mathbb{R}^2$.) Clearly, the codimension of $\mathcal{C}^1$ is insufficient to characterize the type of singular fibers over $\mathcal{C}^1$ and we should consider separately all possible topologically different singular fibers [39], corresponding critical value lines $\mathcal{C}^1$, and their arrangement within the image of the EM map, as well as the structure of the toric fibration near the singular fibers in $\mathrm{EM}^{-1}(\mathcal{C}^1)$. Since monodromy is a topological property this information should in principle be sufficient to define its generalization.

Fractional monodromy. One possibility for a 'crossable' line $\mathcal{C}^1$ of critical values was pointed to by Nekhoroshev and coworkers in [40] (see [22, 24, 41] for more details) who were inspired by the quantum models of [25]. For each point c on such $\mathcal{C}^1$, the singular fiber $\mathrm{EM}^{-1}(c)$ is the 'curled torus' shown in fig. 1, right. The singularity of this fiber consists of one unstable periodic orbit γ_* (while the rest of the variety is a connection of stable and unstable manifolds of γ_*). Assuming that one of the first integrals is the momentum, the singular orbit is a special orbit of the respective circle action which is two times shorter than all other (regular) orbits of this action. In order to be two times longer, these latter orbits 'curl' about γ_*. So we can embed $\mathrm{EM}^{-1}(c)$ in the three-dimensional space as a cylinder on the figure eight whose ends are identified after a halftwist. Such singular fiber and the corresponding line $\mathcal{C}^1$ exists typically in the case of 1:2 resonances [42].

As stated in [40], certain cycles can be continued along the path crossing $\mathcal{C}^1$ because the singularity of the curled tori is of a 'mild' kind. These cycles generate a subgroup of the fundamental group of the torus

which is big enough to define generalized monodromy. However, just existence of a family of curled tori is not sufficient for the system to have monodromy. We also need a special arrangement of the singular and regular values in the image $\mathcal{R}$ of the EM map. The simplest situation occurs when $\mathrm{EM}^{-1}(f)$ has only one connected component for every value f in $\mathcal{R}$ and the latter is itself connected. This means that the line $\mathcal{C}^1$ cuts through $\mathcal{R}$ and ends up at an isolated singular value $\mathcal{C}^0$ without splitting $\mathcal{R}_{\mathrm{reg}}$ into two parts, see fig. 3, right, where $\mathcal{C}^0$ lies at the origin $0 = (0, 0)$. The authors of [40] give a concrete example of the $1 : (-2)$ resonant oscillator system where this situation occurs. They show that such system possesses *fractional monodromy*, called so because its matrix[1] has fractional coefficient $\frac{1}{2}$. We comment on this system in more detail in sec. 5. At present the authors do not know of any reasonable physical examples of molecular systems which show the presence of fractional monodromy. It is possible to find fractional monodromy in systems with special axial symmetries, such as a nondiagonal S^1 symmetry, which acts on the two subspaces in a way similar the action of the $1{:}(-2)$ resonant oscillator. Another possibility may occur in the study of localized oscillations about stable nonlinear normal modes (such as local modes) in a system with three or more vibrational degrees of freedom, see [22, 43–47] and references therein.

Nonlocal monodromy. A different generalization of monodromy can be attempted in a common situation (see sec. 6) where fibers over the line $\mathcal{C}^1$ are 'bitori', or two tori glued together along one of their principal circles, see fig. 1, second left. In this case, $\mathcal{C}^1$ divides $\mathcal{R}_{\mathrm{reg}}$ locally into two regions $\mathcal{R}'_{\mathrm{reg}}$ and $\mathcal{R}''_{\mathrm{reg}}$ with respective regular values f' and f'' such that the preimage $\mathrm{EM}^{-1}(f')$ is connected, while $\mathrm{EM}^{-1}(f'')$ consists of two (or more) connected components. This means that as we follow a regular torus along a path which goes from $\mathcal{R}'_{\mathrm{reg}}$ to $\mathcal{R}''_{\mathrm{reg}}$, this torus becomes a bitorus and then separates into two tori as we cross $\mathcal{C}^1$. Going in the opposite direction, we should follow two tori which fuse together and become one torus. It is instructive to compare this process to the case of fractional monodromy, where on both sides of the $\mathcal{C}^1$ divide the preimage remains a single regular torus.

Like in the case of fractional monodromy, we need more than just a family of bitori in order for a nontrivial robust topological semi-global (i.e., monodromy-like) property of the singular fibration to exist. In particular $\mathcal{C}^1$ can be a segment surrounded by regular values. Then there exist paths which encircle $\mathcal{C}^1$ and remain entirely in $\mathcal{R}_{\mathrm{reg}}$. Such paths are, obviously, not contractible to a point, and the situation is very similar to that of the usual integer monodromy (sec. 3) albeit the singularity is now a segment and not just one critical value. As we explain in sec. 6.1, such *nonlocal monodromy* exists in many systems. Furthermore, one can envisage a continuous deformation of a system with local integer monodromy into the one with nonlocal monodromy [22].

Bidromy. A very different topology, which also involves a family of bitori, is discussed in sec. 6.2. In that case, unlike the previous case of nonlocal monodromy, it seems that the topological characteristics of the singularity should be obtained by crossing $\mathcal{C}^1$. We call such characteristics *bidromy* and we give an example of a situation, where we conjecture that bidromy can be introduced.

Obstructions in higher dimensions. Finally, for $N > 2$, it is possible to suggest more complicated obstructions to the existence of global action-angle variables [1] caused by the presence of isolated sets of critical values of codimension higher than 2. Because in such cases all closed paths in $\mathcal{R}_{\mathrm{reg}}$ are contractible to a point, monodromy is, obviously, trivial. Yet action-angle coordinates cannot be defined globally in $\mathrm{EM}^{-1}(\mathcal{R}_{\mathrm{reg}})$, and this can be indicated by other appropriate topological characteristics of the fibration. Unfortunately, even though several formal models of such singular fibrations are known [48–51], we still do not have any concrete physical examples in atomic and molecular systems. So we do not discuss these generalizations.

[1] Generalized monodromy matrices M belong to $\mathrm{SL}(2, \mathbb{Q})$, i.e., $\det M = 1$ and entries are rational numbers.

2.5 *Quantum monodromy*

We can now turn to quantum manifestations of classical monodromy introduced in the previous section. This is followed in sec. 3, 5, and 6 by several concrete, simple but typical examples of model quantum systems of interest to atomic and molecular physics.

As already mentioned in sec. 2.3, local classical actions $I_1, \ldots, I_N$ give a most direct way to establish the correspondence between the classical Hamiltonian dynamical system and its quantum analog. Notice that on any given regular torus, the values of $I_1, \ldots, I_N$ equal the integrals $(2\pi)^{-1} \oint p dq$ over the circle orbits of the respective flows. On the other hand, according to the well known Einstein–Brillouin–Keller (EBK) principle [34], the values of these integrals for the quantum states should be nonnegative integers $n_1, \ldots, n_N$, or *local quantum numbers*, times[1] $\hbar$ plus certain correction terms $\mu_1, \ldots, \mu_k$ which are related to the properties of the q-space projections of the above orbits and are often called after Maslov. Furthermore, near the classical limit where quantum states are sufficiently dense and manifestations of classical phenomena such as monodromy can be studied, $n_1, \ldots, n_N$ are large and $\mu_1, \ldots, \mu_k$ can be neglected.

The tori on which the EBK conditions are met are called EBK tori. It follows that quantum states of the system can be represented as the image of the EBK tori under the EM map. This image constitutes an N-dimensional lattice of points which lies within the range $\mathcal{R}$ of the EM map. We call this lattice *quantum* EM *eigenvalue lattice* or *integer action lattice*, or simply quantum lattice for brevity. Each node of this lattice represents such values f of first integrals $F_1, \ldots, F_N$ for which the values of local actions $I_1, \ldots, I_N$ are integers[1]. It can be computed as a set of common eigenvalues (or joint spectrum) of N mutually commuting quantum observables $\hat{F}_1, \ldots, \hat{F}_N$ which correspond to classical integrals $F_1, \ldots, F_N$. In order to understand quantum-classical correspondence in a particular system, it is often quite helpful to represent on the same plot both the image of the classical EM map (with its critical and regular values) and the set of common eigenvalues.

From the above quantum-classical correspondence principle and the fact that the classical EM map defines a locally trivial toric fibration it follows immediately that the respective quantum lattice should be a locally regular lattice. Such lattice is locally isomorphic to an abstract $\mathbb{Z}^N$ lattice[2]. Furthermore, any open connected domain of the regular values of EM over which our toric fibration remains trivial should cover regular parts of the quantum lattice, i.e., parts of the lattice which can be deformed smoothly into a $\mathbb{Z}^N$. From a more formal point of view, parts of our quantum lattice can be represented using regular $\mathbb{Z}^N$ *charts* as parts of an ideal lattice.

Of course, if the toric fibration over the entire domain $\mathcal{R}_{\text{reg}}$ of regular values of EM is trivial, then global actions (and hence global quantum numbers) exist everywhere and we need just one $\mathbb{Z}^N$ chart to cover the whole quantum lattice within $\mathcal{R}_{\text{reg}}$. We are interested, however, in integrable systems where precisely the opposite happens, i.e., the fibration is nontrivial. Such systems serve as models of many important atomic and molecular systems (see sec. 1). They do not have global quantum numbers and require several $\mathbb{Z}^N$ charts forming an *atlas* to cover their entire quantum lattice within $\mathcal{R}_{\text{reg}}$.

The necessity to use several charts indicates that the lattice is globally nonregular, i.e., it has one or several *defects*. To characterize these defects we can use a method which is very reminiscent of the techniques used in crystallography. This idea can be traced back to [3], its particularly simple and didactic application called *elementary cell diagram* resurfaced in [6, 7, 9] and since became a very standard tool. Notice that the defects of the nonregular lattices of common quantum eigenvalues which correspond to singular fibrations of classical systems with monodromy differ from those usually considered in physical crystals. For more on the crystallographic analogy see [26].

Classical monodromy manifests as a particular quantum lattice defect. To characterize this defect, we choose an elementary cell of the lattice (typically the smallest possible nearly rectangular cell) in the vicinity of the starting point f^0 on the contour Γ which was used in sec. 2.4 to compute classical monodromy. Since f^0 is a regular EM value, it is covered by one of the local $\mathbb{Z}^N$ charts. Within such chart we can easily move the cell approximately along Γ using the natural parallel transport rules of $\mathbb{Z}^N$ (i.e., by stepping local quantum numbers). We would have to use several charts to complete our tour on Γ, and we would use the

[1]Notice that hereafter we will imply atomic units in which $\hbar = 1$, and neglect semiclassical corrections μ.
[2]$\mathbb{Z}^N$ is an N-dimensional cubic lattice formed by all integers in the space $\mathbb{R}^N$ which in our case is the space of the values of local actions.

rules of going from one chart to the other. Arriving back near point $f^1 = f^0$ and attempting to superimpose the final and the initial cells, we would find that the cells cannot match. Since elementary cells represent the choice of local actions, this comes as no surprise in view of all we have learned about classical monodromy in sec. 2.4. Using an arbitrary basis of the locally regular lattice near $f^1 = f^0$ we can define the transformation between the initial and final cell. This transformation is given by the quantum monodromy matrix, which is an *inverse transpose* of the classical monodromy matrix [23, 24] : $M_{\text{quantum}} = \left(M^{-1}_{\text{classical}}\right)^{\mathrm{T}}$. Like its classical counterpart (see sec. 2.4) it defines monodromy transformation with respect to the chosen initial elementary cell. Since different elementary cells are related among themselves by similarity transformations in $\mathrm{SL}(N, \mathbb{Z})$, quantum monodromy matrix M_{quantum} represents a class of conjugated elements of $\mathrm{SL}(N, \mathbb{Z})$.

3 Quantum monodromy for 1 : (−1) resonance

We describe one of the simplest completely integrable Hamiltonian dynamical systems with two degrees of freedom which possess monodromy. This example system is defined on a four dimensional classical phase space $\mathbb{R}^4_{q,p}$ with coordinates $q = (q_1, q_2)$ and conjugate momenta $p = (p_1, p_2)$ by two Hamiltonian functions in involution

$$F_1 = \tfrac{1}{2}(p_1^2 + q_1^2) - \tfrac{1}{2}(p_2^2 + q_2^2), \tag{1a}$$

$$F_2 = p_1 q_2 + p_2 q_1 + \tfrac{1}{4}\left(p_1^2 + q_1^2 + p_2^2 + q_2^2\right)^2. \tag{1b}$$

From the point of view of the topology of its toric fibration and the image of its EM map, the study of the system defined by (1) is equivalent to the analysis of the motion of a single particle in a two-dimensional axially symmetric potential $V(r) = ar^4 - br^2$ [52,53], often referred as 'champagne bottle' or 'Mexican hat', or to the study of vibrations of a quasi-linear molecule near its unstable linear configuration [11]. In general, the unstable equilibrium of such systems is known in mathematics as *focus-focus singularity* [23,35,36,38].

The image of the EM map defined by the first integrals $F = (F_1, F_2)$ in (1) is shown in fig. 4. The set $\mathcal{R}_{\text{reg}}$ of regular values has the topology of an open half-plane punctured in $f_1 = f_2 = 0$ and bounded from below by a one-dimensional subspace of critical values. The puncture is the isolated critical value 0 which is, as explained in sec. 2.4, at the origin of monodromy. The preimage $\mathrm{EM}^{-1}(f)$ of any regular value f in $\mathcal{R}_{\text{reg}}$ is a two-torus $\mathbb{T}^2_f$; the inverse image of any critical value c on the lower boundary is a periodic orbit $\mathbb{S}^1_c$ (i.e. a one-dimensional torus); the preimage $\mathrm{EM}^{-1}(0)$ of the isolated critical value is a pinched torus. The latter is similar to the fiber shown in fig. 1, second right, and includes the unstable (hyperbolic) equilibrium $q = p = 0$ together with the homoclinic connection of its stable and unstable manifolds.

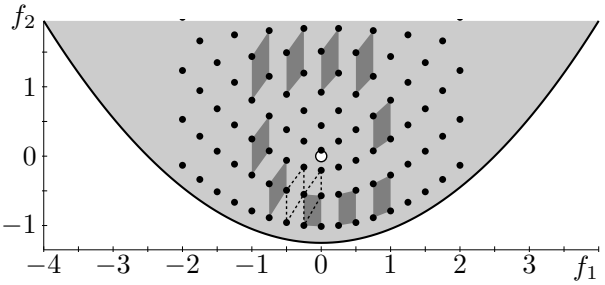

Figure 4. Base of the integrable fibration of the 1:(−1) resonant oscillator system defined by the first integrals F in (1) and the corresponding quantum lattice (black dots). Dark gray quadrangles show the evolution of the elementary cell (w_1, w_2) along the closed path Γ which goes around the isolated critical value (large opaque circle). The set of regular values is shaded light gray.

The system of common eigenvalues (joint spectrum) of quantum operators $(\hat{F}_1, \hat{F}_2)$ corresponding to classical functions in (1), i.e. the quantum lattice of this system, is also shown in fig. 4. We can see that in any simply connected domain of regular EM values this lattice is isomorphic to a regular $\mathbb{Z}^2$ lattice. (Recall that in sec. 2.5 we called such lattice locally regular.) At the same time, the whole lattice requires

an atlas of *two* charts (assuming that each individual chart cannot overlap itself). We demonstrate that in figure 5 which represents one possible choice of such atlas. On each chart shaded gray, we show constant value lines of integer numbers n_1, n_2 labeling the underlying standard $\mathbb{Z}^2$ lattice. As explained in sec. 2.5, these numbers are local quantum numbers which correspond to integer values of local actions. The two charts overlap in a sufficiently large region which allows to express the cell in one chart in terms of the coordinates defined for the alternative chart.

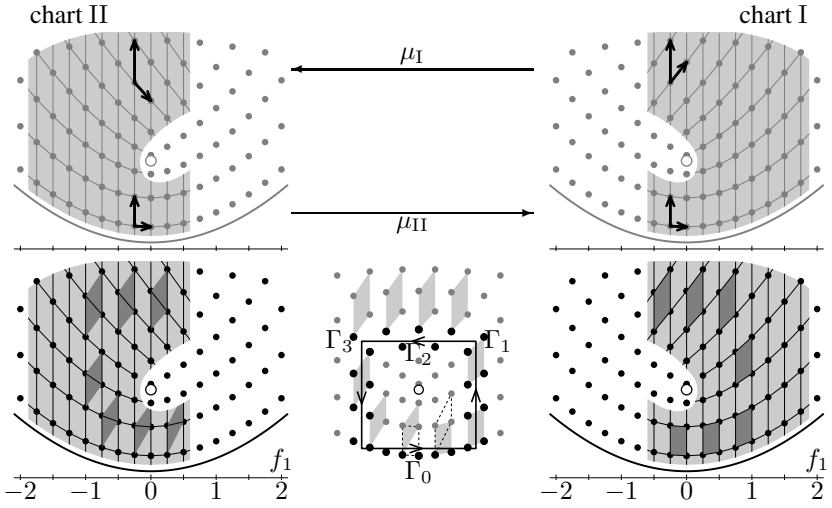

Figure 5. Two-chart atlas (left and right panels) of the quantum lattice of the 1:(−1) resonant oscillator system. Open domains $D_{\rm I}$ and $D_{\rm II}$ are shaded grey; solid lines within these domains join nodes of the corresponding full regular lattices $L_{\rm I}$ and $L_{\rm II}$. Top plots show the choice of basis cells for charts I and II and the gluing maps between the charts; bottom plots show the transport of the elementary cell (dark grey quadrangles) in each chart. Central bottom panel shows contour Γ as a bold solid rectangle and the set $\Gamma^{\rm quant}$ as emphasized black dots.

Of course, other choices of charts are possible. For example, Dixon pointed out long time ago [27, 54] that the low and high energy regions, i.e. upper and lower regions lying roughly below and above $f_2 = 0$, respectively, can be described using two different sets of good quantum numbers. Away from the $f = 0$ singularity, these regions can overlap significantly. It is evident that Dixon's charts are entirely similar to our overlapping left and right charts in fig. 5. In general, not only the choice of charts is ambiguous but also the choice of the basis within each chart (i.e. the choice of the lines forming the rectangular net) can be modified. However, the result of the parallel transportation of a given elementary cell within each chart does not depend on the choice of the basis, and the result of the counterclockwise transportation along any closed path Γ which encircles the critical value 0 once (fig. 4 and 5) does not depend on the choice of the charts.

In particular, it can be seen that we have to use both charts of our atlas in order to transport an elementary cell along Γ. Thus, for example, starting in the lower overlap region on chart I (see fig. 5), the entire cyclic transportation of such cell can be accomplished in the following four steps: (i) propagate the initial cell within chart I till the upper overlap region; (ii) redefine the cell in chart II using the gluing mapping $\mu_{\rm I}$; here the sides of the cell, written in the basis of chart I as $(1, 0)$ and $(0, 1)$, become in the basis of the chart II the sides $(1, 1)$ and $(0, 1)$; (iii) propagate the cell in chart II till the lower overlap region; (iv) redefine the final cell in chart I using the mapping $\mu_{\rm II}$. As soon as the initial and final cells are defined in the same chart, the $\mathrm{SL}(2, \mathbb{Z})$ monodromy matrix for the transformation relating them can be written immediately.

4 Quantum monodromy in systems with three degrees of freedom. Example of the 1:1:2 resonance

In the case of completely integrable Hamiltonian dynamical systems with three degrees of freedom, the image $\mathcal{R}$ of the EM map is three-dimensional (3D). It consists typically of an open 3D domain of regular values $\mathcal{R}_{\rm reg}$, and of subspaces of critical values of codimension one, two and three, which are surfaces, lines,

and points, respectively. In particular, the boundary $\partial\mathcal{R}$ of $\mathcal{R}$ is a set of critical values of codimension-1, i.e. a 2D surface. This boundary can be smooth, or can contain further sets of critical values of codimension two and three. The inverse image of any regular value in $\mathcal{R}_{\rm reg}$ is a three-torus $\mathbb{T}^3$; the fiber over the regular points of $\partial\mathcal{R}$ is a two-torus $\mathbb{T}^2$.

Sets of critical values may also lie *inside* the domain $\mathcal{R}_{\rm reg}$. In particular, consider a line $\mathcal{C}^1$ of critical values which lies inside $\mathcal{R}_{\rm reg}$ and whose ends lie outside $\mathcal{R}_{\rm reg}$. For example, the ends of $\mathcal{C}^1$ can be attached to $\partial\mathcal{R}$ (which is, obviously, not part of $\mathcal{R}_{\rm reg}$) or lie in infinity. In such situation, $\mathcal{C}^1$ can be encircled by a closed path Γ which goes only through regular values of EM and is noncontractible. As a consequence, such system would have monodromy.

We illustrate the specifics of the three-degrees-of-freedom case with monodromy on the example of an integrable approximation to the elastic pendulum (or *swing-spring*) [55–57] with particular resonance 1:1:2 between the frequency of its doubly degenerate swinging or pendular motion and that of totally symmetric nondegenerate springing motion. It is common to use coordinates (x, y) and z to describe pendular and springing oscillations respectively. In these coordinates the lowest order term in the swing-spring hamiltonian is

$$N = \tfrac{1}{2}(q_x^2 + p_x^2) + \tfrac{1}{2}(q_y^2 + p_y^2) + (q_z^2 + p_z^2) = R + (q_z^2 + p_z^2). \tag{2a}$$

Notice that the degeneracy of pendular frequencies is a direct consequence of the SO(2) symmetry with respect to rotations about axis z. For the same reason, the system has one strict first integral

$$L = L_z = q_x p_y - p_x q_y, \tag{2b}$$

which defines the projection of the angular momentum on this axis.

Since L_z generates a circle action, it is a momentum. However, for the 3D energy-momentum map EM we need a second momentum. The latter is not readily available in a typical system but can be introduced in the limit of small oscillations where we can normalize our system with respect to the circle action defined by N. Truncating the normal form at some degree in (q, p) produces a completely integrable approximation with momenta L_z and n and energy H. In the case of the exact resonance, the principal order of H is cubic in (q, p) and contains a single term

$$S = \tfrac{1}{4}\big[\zeta_z(\bar\zeta_x^2 + \bar\zeta_y^2) + \bar\zeta_z(\zeta_x^2 + \zeta_y^2)\big], \quad \text{where} \quad \zeta = q + \mathrm{i}p, \tag{2c}$$

which describes the Fermi interaction of swinging and springing. In a more general situation, we should take into account the detuning of the exact resonance given by the quadratic term R and a higher order quartic term R^2. So introducing parameters (a, b, c) a 'scalar' part h_0, all of which can be functions of momenta (N, L_z), the energy of the normalized and reduced swing-spring system can be expressed as follows

$$H = h_0 - b\,R + a\,S + c\,R^2. \tag{2d}$$

Of course, for a true Fermi system we assume that b and c are much smaller than a. Reducing this system means replacing N and L_z by their respective values (n, ℓ_z) and considering the reduced system with one remaining degree of freedom for each fixed (n, ℓ_z).

The simple mechanical model of such elastic pendulum has many interesting physical analogies [17], and in particular H replicates the effective vibrational Hamiltonian describing the energy level polyads (or *shells*) formed by the Fermi resonant[1] doubly degenerate bending mode and the symmetric stretching mode of a linear triatomic molecule [17, 18]. In fact the CO_2 molecule turned out to be a nearly perfect 'molecular swing-spring' [17]. For a qualitatively adequate description of the vibrational energy level system

[1]Spectroscopists often use abbreviation 1:2 to designate 3-D Fermi systems with doubly degenerate bending mode. This might, however, be confusing, as it does not allow to distinguish the 3-D systems from a 2-D systems with $1:2$ resonance which do not show the presence of monodromy.

of this molecule, we can neglect h_0, b and c in (2d) and consider the simplest Fermi model with $H = S$. Notice that such model hamiltonian can be obtained by a simple restriction (or first order averaging) of the initial hamiltonian to the n-shell. It describes the bulk of the internal polyad dynamics.

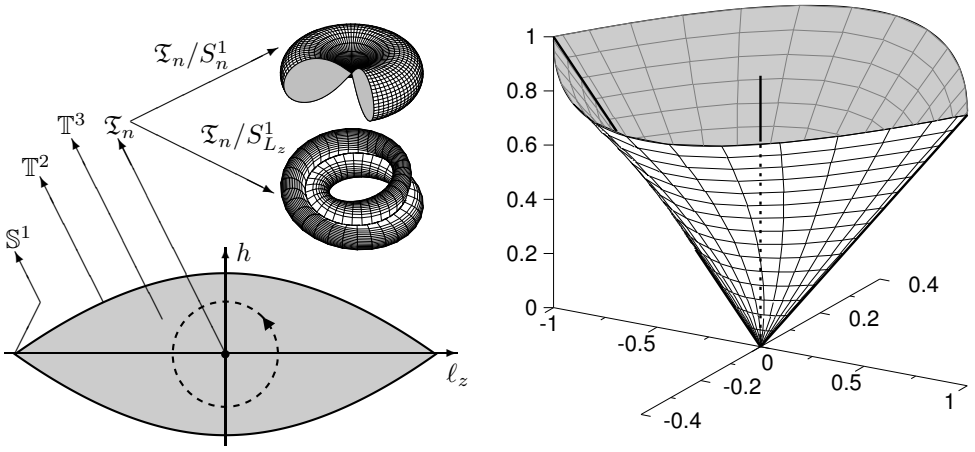

Figure 6. Image of the energy-momentum map EM for the 1:1:2 resonant oscillator system with axial symmetry and $H = S$: full 3D image (right); typical constant-n section of the image and fibers (left)

The image $\mathcal{R}$ of the energy-momentum map EM of an exactly 1:1:2 resonant nonlinear oscillator system with axial symmetry and $H = S$ is represented in fig. 6, right, in coordinates $f = (\ell_z, h, n)$ which correspond to possible values of integrals $F = (L_z, H, N)$. The cone-like boundary $\partial\mathcal{R}$ of $\mathcal{R}$ is a union of two smooth 2D surfaces which are glued together along the two lines $\mathcal{C}^1_\pm$ of critical values $f = (\pm n, 0, n)$. These lines are part of the set of critical values of codimension-2. The critical point $f = 0$, where they meet, is the 'vertex' of $\partial\mathcal{R}$ and constitutes the critical set of codimension-3. Apart from critical values on $\partial\mathcal{R}$ there exists a singular line $\mathcal{C}^1_0$ of singular values $f = (0, 0, n)$ with $n > 0$ which we can represent as a vertical 'thread' inside the 'cone' and which lies inside the domain $\mathcal{R}_{\rm reg}$ of regular values. The latter occupies, of course, the interior of the cone without the thread.

The inverse images $\mathrm{EM}^{-1}(f)$ of the regular values f are regular 3-tori $\mathbb{T}^3_f$, those of the regular part of the 2D boundary are 2-tori. The fiber over points on $\mathcal{C}^1_\pm$ is a special stable periodic orbit, on which L_z achieves its maximum or minimum value at given fixed n. (The corresponding motion of the swing-spring is a cyclic rotation without springing.) The preimage $\mathrm{EM}^{-1}(0)$ of the vertex 0 is the equilibrium point 0 in $\mathbb{R}^6$.

Reconstruction of the inverse images $\mathrm{EM}^{-1}(c)$ of critical values c on the singular thread $\mathcal{C}^1_0$ is less trivial, see fig. 6. The whole of $\mathrm{EM}^{-1}(c)$ is a singular 3-torus $\mathfrak{T}_n$ which can be considered as both 'pinched' and 'curled'. It includes a special 'short' unstable periodic orbit. In the swing-spring this orbit corresponds to pure springing, in CO_2 it is pure symmetric stretch; due to the resonance 1:2, its period is two times shorter than that of other (regular) orbits. As represented in fig. 6, left, reduction of the 3D singular variety $\mathfrak{T}_n$ with respect to the circle action defined by L_z or N gives a 2D pinched torus or a 2D curled torus respectively.

It is clear that any closed path Γ which goes around the thread in the domain of regular values $\mathcal{R}_{\rm reg}$ is noncontractible and leads to nontrivial monodromy. Since the toric fibration of our system is locally trivial, over a sufficiently small neighbourhood of any regular value and in particular, of any point on Γ, we can define local actions. For the quantum system this means that the spectrum of common eigenvalues of operators $(\hat{L}_z, \hat{H}, \hat{N})$ can be mapped locally onto a regular 3D-integer lattice, i.e. a local 3D chart. However, in the presence of monodromy, several such regular lattice charts, each with its own naturally defined parallel transport of elementary cells across it, are required to cover Γ [18]. As discussed in sec. 2.5, we characterize quantum monodromy by following the evolution of an initially chosen elementary 3D cell along Γ. Since cells are translated straightforwardly within each chart, all we have to consider is how our cell transforms when we switch charts. Details for the concrete example of the 1:1:2 resonance can be found in [18].

The 3×3 monodromy matrix M of our system depends naturally on the choice of the basis of the 3D lattice chart in which the initial and the final cells are compared. In a new basis, the monodromy matrix is obtained by the similarity transformation AMA^{-1}, where A is a 3×3 matrix in the $\mathrm{SL}(3,\mathbb{Z})$ group which defines the basis change. In particular, matrices

$$\begin{pmatrix} 1&0&0\\ 1&1&0\\ 0&0&1 \end{pmatrix} \sim \begin{pmatrix} 1&0&0\\ 1&1&-1\\ 0&0&1 \end{pmatrix} \sim \begin{pmatrix} 1&0&0\\ 2&1&1\\ 0&0&1 \end{pmatrix} \sim \begin{pmatrix} 1&0&0\\ 2&1&-1\\ 0&0&1 \end{pmatrix} \sim \begin{pmatrix} -1&-2&1\\ 2&3&-1\\ 0&0&1 \end{pmatrix} \tag{3}$$

are all equivalent up to such transformation and represent, each with respect to a different basis and therefore a different initial elementary cell, the same monodromy transformation μ_Γ for the evolution of the cell along the path Γ which encircles the thread of singular values of the 1:1:2 system. Dependence of M on the choice of the basis must be taken into account if one studies the evolution of a 2D cell along a closed path in a 2D section of the full 3D quantum lattice. Thus within any constant n section we find that in a suitable basis of the 2D sublattice the 2×2 monodromy matrix equals $\left(\begin{smallmatrix} 1&0\\ 2&1 \end{smallmatrix}\right)$, whereas for any section with constant $n+l_z$ this matrix is of the form $\left(\begin{smallmatrix} 1&0\\ 1&1 \end{smallmatrix}\right)$.

Another important observation, which can be done on the example of the 1:1:2 resonant oscillator system, concerns the *structural stability* or the *persistence* of monodromy under small deformations which preserve the symmetry and the integrability of the system. One such deformation of our simple $H = S$ model can be produced by adding a small term $-b\,R$ in (2d) which describes detuning of the frequencies of the double degenerate mode (swinging) and the nondegenerate mode (springing) from the exact ratio 1:2. In molecular applications where the 1:2 degeneracy is always only approximate [19, 58–60], such generalization of the $H = S$ model is both physically reasonable and natural. It can be shown that for $b \neq 0$ (and typically small) the image of the EM map in the region of sufficiently large n values remains unchanged and the isolated thread of critical values persists there. On the other hand, at n near a certain small critical value, even a tiny perturbation, such as $c\,R^2$ in (2d) with small $c \ll a$ can cause qualitative changes because the position of the point where the thread $\mathcal{C}^1_0$ branches off the boundary $\partial\mathcal{R}$ can change continuously even under very small perturbations. We will analyze such modifications in sec. 6.2.

5 Fractional monodromy in the 1:(−2) resonance

Recall from sec. 2.4 that standard or integer Hamiltonian monodromy [1] is defined as a transformation of local actions (or basis cycles on regular tori) associated with the closed path Γ which lies entirely in the domain $\mathcal{R}_{\mathrm{reg}}$ of regular values of the EM map. Generalization of this concept was suggested recently in [24, 40]. It allowed for more general paths which can cross certain lines $\mathcal{C}^1$ of critical values in the range of the EM map and resulted in the definition of fractional monodromy [22, 24, 25, 40, 41]. As we already pointed out, this generalization was possible due to a relatively 'mild' singularity of the curled tori (rightmost in fig. 1), which are the fibers $\mathrm{EM}^{-1}(c)$ over critical values c in $\mathcal{C}^1$. Such singularity allows to continue a large subset of cycles across $\mathcal{C}^1$ and these latter generate a finite-index subgroup ζ of the fundamental group of the torus $\pi_1(\mathbb{T}^2)$. The subgroup ζ is complete in the sense that like the $\pi_1(\mathbb{T}^2)$ group itself, ζ is isomorphic to an abstract integer lattice $\mathbb{Z}^2$. Restricting the analysis to ζ, we can 'cross' $\mathcal{C}^1$.

In quantum mechanics, this restriction is equivalent to the restriction of the lattice of quantum states to a certain *sublattice* and the possibility to study the evolution of a *multiple* cell along Γ. Contrary to an elementary cell, such multiple cell can be transported across $\mathcal{C}^1$ independently on the point of crossing.

We illustrate quantum fractional monodromy on the example of the quantum state lattice of the 1:(−2) resonant nonlinear oscillator system introduced in [40]. This two-degree-of-freedom completely integrable system is defined by two classical Hamiltonian functions in involution

$$F_1 = \tfrac{1}{2}(p_1^2 + q_1^2) - (p_2^2 + q_2^2), \tag{4a}$$

$$F_2 = 2p_1q_1q_2 + q_1^2\,p_2 - p_1^2\,p_2 + \tfrac{1}{4}\big(p_1^2 + q_1^2 + 2p_2^2 + 2q_2^2\big)^2. \tag{4b}$$

As we can see from (4a), this system represents two non-linear oscillators whose frequencies are in the 1:(−2) resonance. The image $\mathcal{R}$ of the classical EM map defined by (4) together with the superimposed joint spectrum of two corresponding commuting quantum observables $(\hat{F}_1, \hat{F}_2)$ is shown in fig. 7. It can

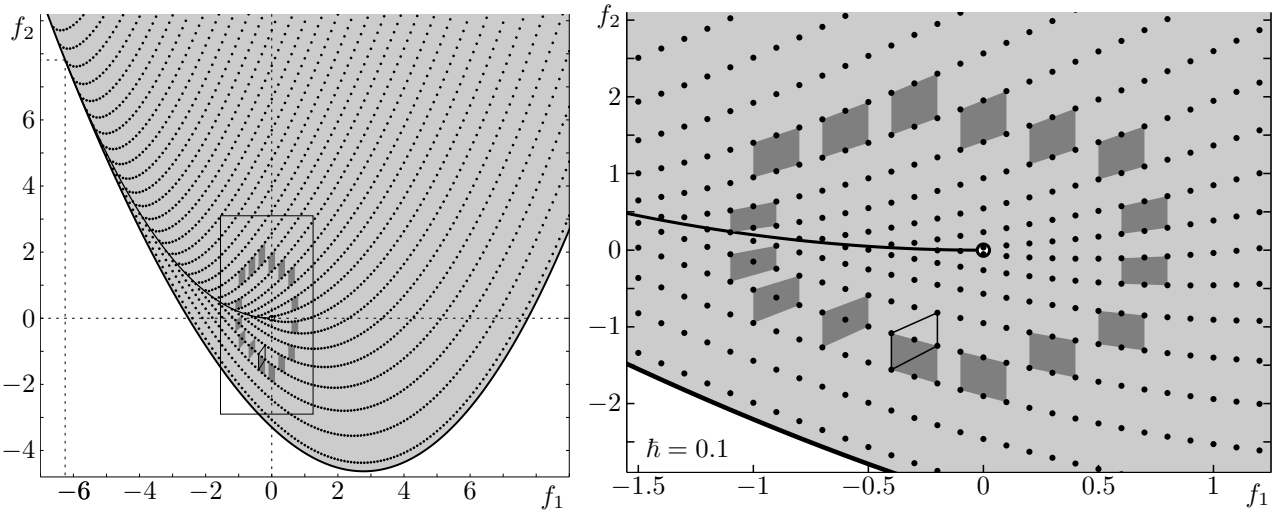

Figure 7. Lattice $L^{1:(-2)}$ of quantum states in the base space (shaded area) of the integrable fibration F of the 1:(−2) resonance oscillator. Bold lines represent critical values of F: relative equilibria (lower boundary) and weak singular values; the singular value at $(0, 0)$ is marked by a large opaque circle. Dark gray quadrangles show the evolution of the minimal cell of the index-2 sublattice along the closed path Γ which goes around $(0, 0)$.

be seen that $\mathcal{R}$ includes a 2D region $\mathcal{R}_{\text{reg}}$ of regular values and that the latter is simply connected and bounded from below by a smooth boundary line $\partial\mathcal{R}$ of critical values. Another line of critical values $\mathcal{C}^1$ lies *inside* the domain $\mathcal{R}_{\text{reg}}$ and is 'attached' at one end (left in fig. 7) to $\partial\mathcal{R}$. The other end of $\mathcal{C}^1$ is the isolated 'strong' critical value $0 = (0, 0)$. The situation near 0 is similar to that in fig. 3, right.

The preimage of each regular value in $\mathcal{R}_{\text{reg}}$ is a single two-torus. Each point in $\partial\mathcal{R}$ lifts to a single periodic orbit. For each point c on $\mathcal{C}^1$ the inverse image $\text{EM}^{-1}(c)$ is a curled torus. Similar to $\mathfrak{T}$ in sec. 4, the singular circle of this 2D fiber is a special short periodic orbit of the flow generated by F_1 in (4a) which lies in the plane $\{q_1 = p_1 = 0\}$.

For all joint quantum eigenvalues which lie in $\mathcal{R}_{\text{reg}}$ outside a small open neighbourhood of $\mathcal{C}^1$, 0 and, of course, the boundary $\partial\mathcal{R}$, the quantum state lattice of the 1:(−2) system can be mapped entirely to a single regular integer lattice $\mathbb{Z}^2$. However, crossing the singular line $\mathcal{C}^1$ cannot be defined in an unambiguous way for an elementary cell of this lattice. At the same time, if we consider an index-two sublattice by selecting nodes which correspond either to only even or to only odd eigenvalues of L, we can construct a local regular chart of such sublattice which covers $\mathcal{C}^1$ and its neighbourhood but *not* 0 and its neighbourhood—see chart II in fig. 8, left. The elementary cell of such sublattice is a *double cell* of the initial lattice. To cover a closed path Γ which goes around 0 and crosses $\mathcal{C}^1$, we also need chart I (fig. 8, right) which covers only regular values and can be defined straightforwardly. The two charts form the atlas of the singular index-2 sublattice. Using this atlas we can transport a double cell (the elementary cell of the sublattice) along Γ and therefore to compute a monodromy matrix for a sublattice in a standard way.

The transport of the double cell is illustrated in fig. 8. It can be seen that crossing of the singular line within chart II is unambiguous. Notice that before and after the crossing, the representation of such double cell in terms of elementary cells differs. As soon as the initial and final cell belong to the same regular chart, we can define the monodromy transformation for the double cell and compute its matrix $\left(\begin{smallmatrix} 1 & 0 \\ 1 & 1 \end{smallmatrix}\right)$ for the particular basis choice in fig. 8. Extending this transformation *formally* to elementary cells, we get the monodromy matrix $\left(\begin{smallmatrix} 1 & 0 \\ \frac{1}{2} & 1 \end{smallmatrix}\right)$ with a half-integer entry. We note that similar to ordinary integer monodromy, fractional monodromy does not depend on the choice of local charts and on the choice of Γ (within the class of homotopically equivalent paths). Neither does it depend on the point where Γ crosses $\mathcal{C}^1$.

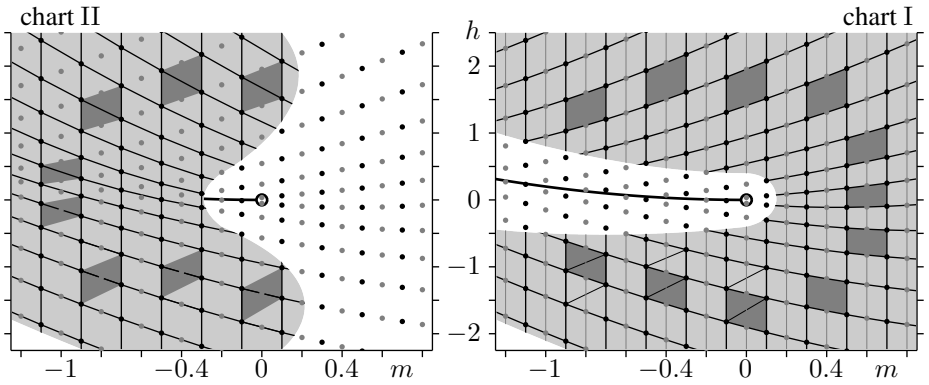

Figure 8. Two-chart atlas of the quantum lattice of the 1:(−2) resonant oscillator system. Open domains $D_{\rm II}$ (left) and $D_{\rm I}$ (right) are shaded grey; black dots and lines joining them within these domains correspond to the common sublattice of index 2; faded lines and dots represent the complementary sublattice in the full lattice chart I.

6 Qualitative features of fibrations with several disconnected fibers

In this section we consider integrable systems with N degrees of freedom whose EM map has an open N-dimensional domain of regular values f such that the preimage $\mathrm{EM}^{-1}(f)$ consists of several disconnected components. We call the latter fibers. Naturally, since f are regular values, the fibers are regular N-tori.

To have a simple example, consider $N = 2$ and let $\mathcal{R}_1$ and $\mathcal{R}_2$ be such two open domains within the domain $\mathcal{R}_{\rm reg}$ of all regular values of EM, that the preimage $\mathrm{EM}^{-1}(a)$ of any value a in $\mathcal{R}_1$ has one connected component (fiber), for as $\mathrm{EM}^{-1}(b)$ for any b in $\mathcal{R}_2$ consists of *two* fibers. We assume that $\mathcal{R}_{\rm reg}$ is a union of $\mathcal{R}_1$ and $\mathcal{R}_2$, and we call the latter single component and two-component *lower cell* respectively. Notice that the inverse image $\mathrm{EM}^{-1}(\mathcal{R}_1)$ of $\mathcal{R}_1$ is part of a single *upper cell*, while the preimage $\mathrm{EM}^{-1}(\mathcal{R}_2)$ belongs to two nonoverlapping (i.e. disjoint) upper cells. (For more about lower and upper cells, see [24].)

The boundary $\partial\mathcal{R}_2$ of the two-fiber cell $\mathcal{R}_2$ can be formed by different lines of critical values. We can classify such lines by following the metamorphosis of the fibers in $\mathrm{EM}^{-1}(b)$ as b approaches $\partial\mathcal{R}_2$ transversely from within $\mathcal{R}_2$. There can be lines of critical values c for which as $b \to c$, one of the fibers in $\mathrm{EM}^{-1}(b)$ degenerates to a circle, while the other remains a regular 2-torus. We call such lines *degeneracy lines*. Of course, it is possible for both fibers to degenerate simultaneously, but this is atypical. A different possibility is for both regular fibers in $\mathrm{EM}^{-1}(b)$ to merge together into one singular fiber called *bitorus* (or two tori glued together along a circle which is a hyperbolic periodic orbit, see fig. 1, second left). The boundary line for which this happens, separates $\mathcal{R}_1$ and $\mathcal{R}_2$ so that after the two components merge into a bitorus, we can move into $\mathcal{R}_1$ and the bitorus becomes a single regular 2-torus. This situation is illustrated in fig. 9. We call such boundary line a *merger line*.

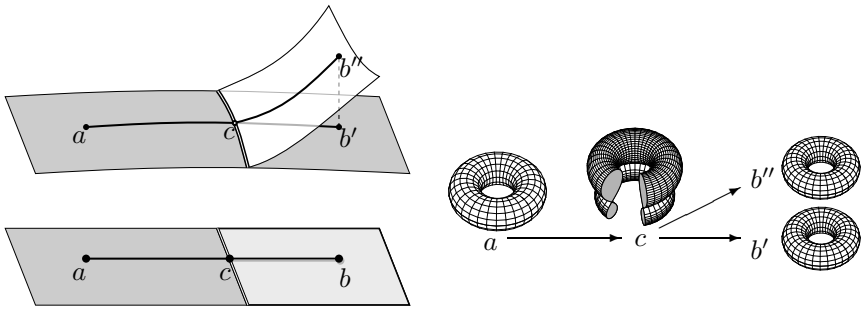

Figure 9. Example of overlapping lower cells in the 2D-image of the energy-momentum map : a multi-sheet cell unfolding surface (top left) and the corresponding EM image (bottom). Points a, b', b'', and c lift each to one connected component of the integrable fibration shown right; b' and b'' correspond to the same EM value b.

As can also be seen from fig. 9, the image of the EM map with multi-component lower cells can be represented using a *cell unfolding surface*. Any point on such surface lifts to a single fiber. Thus a point

b in the two-component region $\mathcal{R}_2$ is represented by two points b' and b'' on the unfolding surface. It is clear that degeneracy lines become boundaries of the unfolding surface. On the other hand, merger lines become singular branching lines of this surface. Thus the unfolding surface in fig. 9, top left, consists of three leafs glued together along one merger line $\mathcal{C}$.

Several arrangements of $\mathcal{R}_1$ and $\mathcal{R}_2$ within $\mathcal{R}_{\rm reg}$ are possible. Their classification can be attempted on the basis of different possible positions of the merger line (or segment) $\mathcal{C}$ with respect to $\mathcal{R}_{\rm reg}$. Thus it is possible that $\mathcal{C}$ divides $\mathcal{R}_{\rm reg}$ into two parts as shown in fig. 9, bottom left. In such a case, we must cross $\mathcal{C}$ in order to connect any of the regular values a, b', and b'' which belong to different sheets of the unfolding surface. Other possibilities include cases illustrated in fig. 10 and 11 where one or both end points of $\mathcal{C}$ lie *inside* $\mathcal{R}_{\rm reg}$. Notice that the singular fiber over such 'internal' endpoint is a singular (nonsmooth) 2-torus in fig. 1, left, which can be regarded as a bitorus with one of its Siamese twin tori contracted to a circle.

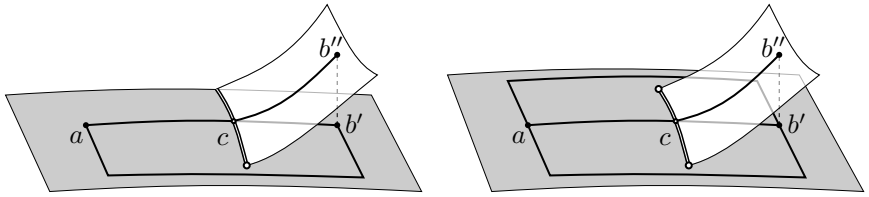

Figure 10. Possible two-sheet cell unfolding surfaces for the image of an EM map with two overlapping lower cells. Fibers in the image of EM^{-1} can have either one (a) or two (b' and b'') connected components; a and b' can be related by a continuous path which lies in the set of regular EM values of the "lower" (grey) sheet. In the case of the right surface, this sheet is not simply connected and the system has monodromy.

In both cases shown in fig. 10, the unfolding surface has two leafs. Especially interesting is the situation in fig. 10, right, where $\mathcal{C}$ is a segment which lies inside the domain of regular values $\mathcal{R}_{\rm reg}$. As a result, one of the leafs in this case is multiple connected and $\mathcal{C}$ can be encircled by a closed noncontractible path Γ consisting entirely of regular value points of this leaf. This means that such system should have monodromy associated with the class of closed paths homotopic to Γ. Furthermore, this monodromy can be introduced in a standard way using an atlas of local charts of the leaf in question. We call such monodromy *nonlocal* because the obstacle $\overline{\mathcal{C}}$ encircled by Γ has non-zero dimension. A concrete example follows in sec. 6.1.

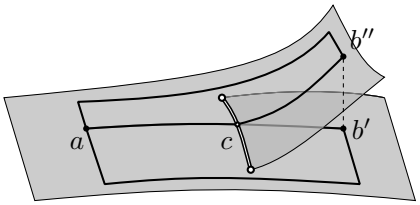

Figure 11. A single-sheet cell unfolding surface for the image of an EM map with one self-overlapping lower cell: the inverse map EM^{-1} can have one (point a) or two (points b' and b'') connected components.

A qualitatively different topology is shown in fig. 11. Similar to fig. 10, right, the closed merger segment $\overline{\mathcal{C}}$ (i.e. $\mathcal{C}$ with both its endpoints) lies entirely inside $\mathcal{R}_{\rm reg}$. However, the unfolding surface now has *one* self-overlapping leaf which is connected (and even simply connected). More specifically, despite the fact that there is a two-component region $\mathcal{R}_2$ (the overlap region of the unfolding surface), any two points b' and b'' of the unfolding surface associated with the same point b in the image of the energy-momentum map EM and any regular value a in the one-component region of this image can be now connected by a continuous path Γ going only through regular points of the unfolding surface. This means that the regular torus $\mathbb{T}^2_a = \mathrm{EM}^{-1}(a)$ and the two components $\mathbb{T}^2_{b'}$ and $\mathbb{T}^2_{b''}$ of $\mathrm{EM}^{-1}(b)$ can be all interconnected by a continuous path in the phase space $\mathbb{R}^4_{q,p}$ which crosses *only* regular tori.

Consider now a closed continuous path Γ which encircles $\overline{\mathcal{C}}$ in the image of the EM map and includes the regular values a and b. Although Γ is a closed curve in the image of the EM map, it is not closed on the unfolding surface—it starts in b' and ends in b'' as shown in fig. 11. Furthermore notice that when entering and leaving the two-component region $\mathcal{R}_2$, the path Γ crosses singular value lines in the image of

EM. These lines are degeneracy lines which define the boundary of the unfolding surface. After unfolding, Γ consists only of regular points; the respective path in $\mathbb{R}^6_{q,p}$ crosses only regular tori.

Existence of such path suggests that it might be possible to 'transport' basis cycles of the regular tori (as well as corresponding local actions and elementary cells of the quantum lattice) directly *across* the bitorus (i.e. the hyperbolic singular fiber over the points in $\mathcal{C}$). To this end we should establish the correspondence between the cycle basis on the regular torus $\mathbb{T}^2_a$ and the cycle bases on the two disconnected regular torus components $\mathbb{T}^2_{b'}$ and $\mathbb{T}^2_{b''}$ on the 'other side' of the bitorus. In the image of the EM map this corresponds to going from a to b directly across $\mathcal{C}$, an action which could not be defined in a path-independent way in any of the situations in fig. 9 and 10.

Transporting the cycle basis on $\mathbb{T}^2_a$ across the bitorus means, obviously, branching it into two separate bases, one on $\mathbb{T}^2_{b'}$ and the other on $\mathbb{T}^2_{b''}$. Then without crossing the bitorus (and any other singularities) again we can further transport each of these two bases *back* to the initial regular torus $\mathbb{T}^2_a$. On the unfolding surface, this corresponds to following Γ from b' to a and from b'' to a. Arriving in a, we should merge the two final bases and compare the result with the initial basis on $\mathbb{T}^2_a$. For the complex path which starts in a, goes to the critical value c on $\mathcal{C}$, and then splits in two paths $cb'a$ and $cb''a$ going back to a, this defines a basis transformation for a complete subgroup generated by the cycles on $\mathbb{T}^2_a$. Our conjecture is that within the class of homotopically equivalent paths, such transformation does not depend on the concrete path used for its definition and we call it tentatively *bidromy* transformation. We also conjecture that similar to monodromy, *bidromy* is a structurally stable property of the system. A rigorous mathematical theory of bidromy has yet to be developed and is, obviously, beyond the scope of this paper. We only provide in sec. 6.2 a concrete example of a system with bidromy.

6.1 *Nonlocal monodromy of the quadratic spherical pendulum and nonrigid triatomic molecules*

Nonlocal monodromy has been uncovered in nonrigid triatomic molecules with rigid diatom core, in particular LiNC [15, 16]. The image of the classical EM map for this molecule is given by the values of the vibrational angular momentum ℓ and the energy h. This image and the joint eigenvalue spectrum of the corresponding two commuting quantum operators is presented in fig. 12, right. It can be seen that this system is analogous to the one with the two-leaf unfolding surface in fig. 10, right. The larger leaf is related to the LiNC equilibrium with $(\ell, h) = 0$, the smaller triangular leaf represents the LiCN states. The leafs are glued along the upper boundary $\mathcal{C}$ of the smaller leaf. In the two-component region $\mathcal{R}_2$, we can distinguish two overlapping regular quantum $\mathbb{Z}^2$ lattices, which correspond to the LiNC and LiCN states. As illustrated by an elementary cell diagram in fig. 12, quantum nonlocal monodromy with matrix in the class $\left(\begin{smallmatrix} 1 & 0 \\ 1 & 1 \end{smallmatrix}\right)$ can be defined for a path which encircles the 'cut' $\mathcal{C}$ on the LiNC leaf.

Nonlocal monodromy is relatively well studied in model mathematical systems, such as the family of quadratic spherical pendula [22]. The spherical pendulum is one of the first mechanical systems where classical Hamiltonian monodromy was discovered [3–5, 61]. Its EM map with one isolated critical value point, is shown in fig. 12, top left. The preimage of this critical point is the celebrated isolated singular fiber called *pinched torus* [5,61] shown in fig. 1, second right. The singular point of this fiber corresponds to the unstable (upper) equilibrium known generally as *focus-focus* point [23, 38]. By the geometric monodromy theorem [37, 61], the presence of the pinched torus signifies nontrivial monodromy of the toric fibration in its neighbourhood, and hence of the corresponding quantum lattice. A LiNC-like system is obtained by such quadratic deformation of the spherical pendulum that makes both the lower and the upper equilibrium stable. This deformation blows up the pinched torus into a family of bitori (fig. 1, second left) which begins and ends in cusped tori (fig. 1, left), and which divides the phase space $\mathbb{R}^4$ into two disconnected regions filled with regular tori. In the image of the EM map this corresponds to transforming the single critical value into a critical segment $\mathcal{C}$ with the attached two-component region $\mathcal{R}_2$. It can be shown that this happens as a result of degenerate Hamiltonian Hopf bifurcation [22, 62]. It has also been shown in [16] that further deformations can result in a qualitatively different system with three-leaf unfolding surface in fig. 12, bottom left, and fig. 9. Such system is analogous to the HCN molecule and it does not, of course, have monodromy.

To emphasize the difference from bidromy, which is discussed in sec. 6.2 below, we notice again that the

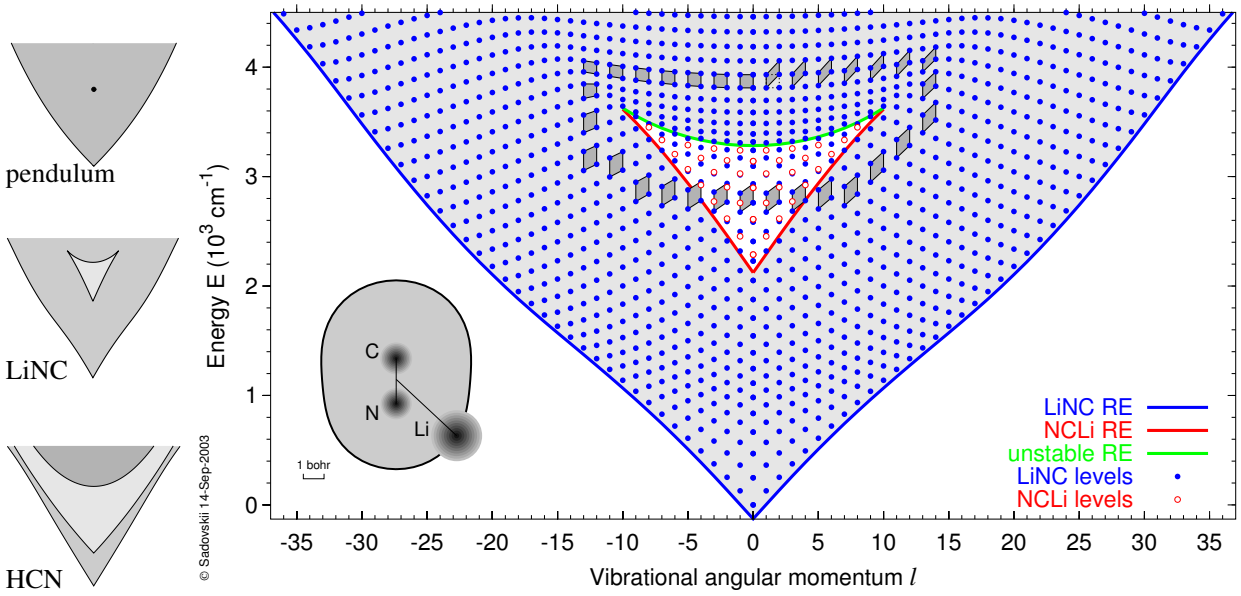

Figure 12. Image of the energy-momentum map EM, quantum lattice, and elementary cell diagram proving nonlocal quantum monodromy for the LiNC molecule (right). Three typical EM images (left): spherical pendulum with one isolated critical value that corresponds to a focus-focus point (top), quadratic spherical pendulum and its molecular realization LiNC with a compact region of values which lift to two disconnected regular fibers, HCN type molecule with noncompact two-fiber region (bottom).

image of the EM map in fig. 12, right, has a two-fiber region. The two regular fibers, which correspond to the same EM value in this region, cannot be connected in the phase space $\mathbb{R}^4$ by a path crossing only regular 2-tori. On the respective unfolding surface, the two points cannot be connected without crossing the merger line $\mathcal{C}$ (recall fig. 10). At the same time, a closed path Γ, which remains on one of the leafs of this surface and which consists of regular points only, can pass around $\overline{\mathcal{C}}$ and can be used to define the nonlocal monodromy. By the deformation argument related to the local or semi-local character of the Hamiltonian Hopf bifurcation in the energy-momentum domain, the nonlocal monodromy should be the same as the usual 'local' monodromy of the parent system before the bifurcation.

6.2 *Bidromy of the detuned* 1:1:2 *resonance*

In sec. 4 we analyzed the simplest possible model of the 1:1:2 resonant swing-spring system, that with energy H equal S (2c), i.e. with $b = 0$ and $c = 0$ in the normalized Hamiltonian (2d). Here we consider a more realistic system with nonzero small b and c, such that $|b| \ll a$ and $|c| \ll a$. Recall that b gives detuning of the 1:2 frequency ratio of the doubly degenerate pendulum oscillation and the non-degenerate swinging modes, which correspond to bending and symmetric stretching of CO_2. In a particular domain of the parameter values b and c, the image EM map of such simple generalized model (2d) and its unfolding has a very interesting nontrivial topology which suggests bidromy.

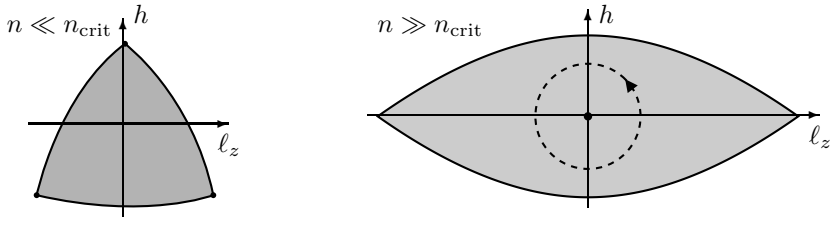

Figure 13. Typical constant-n sections of the image of the energy-momentum map EM for the detuned 1:1:2 resonant oscillator system.

The possibility for new qualitative features in the image of the EM map of the system with Hamiltonian (2d) compared to that of the $H = S$ system studied in sec. 4, follows from the following simple argument.

Let us think for a moment about the classical system. Notice that the detuning term R is of order n^2 while the principal Fermi coupling term S is of order n^3. Therefore, for any even very small detuning $b > 0$, we can find sufficiently low $n < n_{\rm crit}$ for which detuning will be more important than coupling. As a consequence, at such small $n \sim 0$, the constant n section of the 3D-image of the EM map should consist of a simply connected 2D region of regular values whose boundary $\partial\mathcal{R}$ has three exceptional critical values which represent stable relative equilibria (or nonlinear normal modes of the 1:1:2 oscillator in the presence of axial symmetry): the purely springing oscillation with $\ell_z = 0$ and two swinging 'rotations' with maximal and minimal $\ell_z = \pm n$, see fig. 13, left. At the same time, at sufficiently large $n > n_{\rm crit}$, the detuning term $b\,R$ is small in comparison to the Fermi term $a\,S$ and can be neglected. At such large n, the constant n section of the image of the EM map should be qualitatively the same as that of the $H = S$ system in fig. 6, left, which has an isolated singular value inside the region of regular values.

This means that at or near some critical value of $n = n_{\rm crit}(b/a)$, the $\ell_z = 0$ vertex of the EM image in fig. 13, left, should detach from the boundary and move inside the set of regular values $\mathcal{R}_{\rm reg}$. The corresponding relative equilibrium looses stability and the fiber represented by the new isolated critical point is a singular 3D variety $\mathfrak{T}_n$ already described in sec. 4 and fig. 6. For the full 3D image of the EM map, this means that the singular thread which passes inside $\mathcal{R}_{\rm reg}$ for $n \gg n_{\rm crit}$ does not begin in 0 as it is the case for the $H = S$ system whose energy-momentum map is illustrated in fig. 6, right. Instead, this thread branches off the $\ell_z = 0$ edge of the boundary of $\mathcal{R}_{\rm reg}$ when n equals $n_{\rm crit}$. (Notice that $n_{\rm crit} = 0$ for the $H = S$ system.)

The transition from the low-n nonresonant regime to the high-n Fermi resonant structure involves a bifurcation which is reminiscent of the Hamiltonian Hopf bifurcation [8, 22, 46, 62]. The associated change of the geometric structure of the constant n sections of the EM image is very profound and it is quite possible that in the transition interval of n close to some critical value $n_{\rm crit}$, the sections may go through intermediate nontrivial structures and there may be other additional bifurcations. So there is a possibility for the geometry of the 3D image for n close to $n_{\rm crit}$ to be highly nontrivial. We use the term *scenario* to characterize such complex sequences of related bifurcations and structures which are 'organized' by variation of a single parameter n.

Similar to the study of the Hamiltonian Hopf bifurcation [22, 62], we need to take higher order terms into account in order to analyze possible typical (and hence independent on small modifications of the system) transformations of the classical toric fibration and the corresponding quantum spectrum lattice which occur at $n \sim n_{\rm crit}$. The R^2 term in the model system with Hamiltonian H in (2d) is sufficient for this purpose. After neglecting constant terms $h_0(n, \ell_z)$ and rescaling suitably the energy H and the dynamical variables (q, p), we can rewrite the 1:1:2 resonant Hamiltonian (2d) as

$$H = S - R + \frac{1+y}{2}R^2, \tag{5}$$

where y is the only remaining parameter of the rescaled system. In order to represent the image of the EM map in the $\mathbb{R}^3$ space with coordinates (ℓ_z, h, n), we should complement (5) by relation

$$S^2 = (R^2 - L^2)(1 + x - R), \tag{6}$$

where $x = n - n_{\rm crit}$ stands for a small deviation from $n_{\rm crit}$. This relation defines reduced phase spaces $P_{n\ell_z}$ for fixed values of the polyad integral $n > 0$ and vibrational angular momentum L_z,

Similar to the Hamiltonian Hopf bifurcation which has two possible scenarios [8, 22, 46, 62], the scenario of the bifurcation which happens when $x = 0$ depends on the value of the parameter y in equation (5). We retain the terminology in [22, 62] to describe these scenarios.

When $y < 0$ the bifurcation is *supercritical*. For $x < 0$ all constant x sections of the 3D image $\mathcal{R}$ of the EM map are of the 'nonresonant' type in fig. 13, left. The boundary $\partial\mathcal{R}$ of the image $\mathcal{R}$ has three edges. As x varies near $x = 0$ and changes sign from negative to positive, the critical value which formed the $\ell_z = 0$ edge of $\partial\mathcal{R}$ enters inside the domain $\mathcal{R}_{\rm reg}$ of regular values and forms a singular thread inside this domain. The boundary $\partial\mathcal{R}$ for $x > 0$ has two edges. Nothing else happens.

The *subcritical* scenario occurs for $y > 0$ and is (like its Hamiltonian Hopf analog) more complicated.

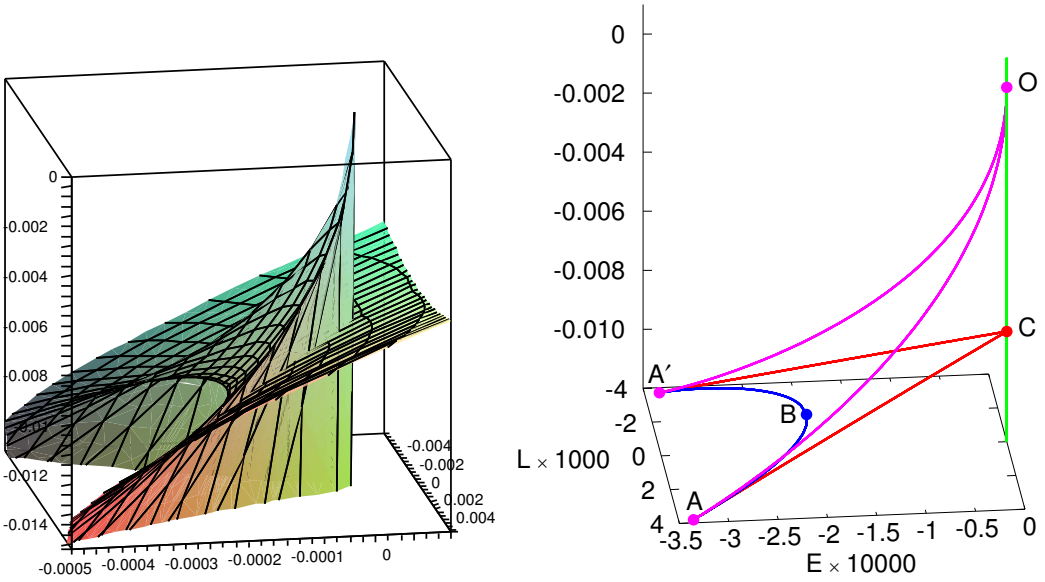

Figure 14. On the left: Part of the self-overlapping boundary of the 3D-image of the energy-momentum map EM for a model of slightly detuned 1:1:2 resonance described by eqs. 5 and 6 with $y = 1/10$ in coordinates (E, L, x). Regular EM values lie left and above the boundary. Inverse EM images of points inside the swallow-tail-like 3D-region have two disconnected components. On the right: Singular lines in the image of the map EM which give a contour (edges) of the swallow-tail-like region. Values of EM which correspond to the second order touching of the constant energy level set and the reduced phase space correspond to AO, $A'O$, and ABA' lines; AC and $A'C$ indicate self-intersection of the boundary; OC line corresponds to the main singularity of the 1:1:2 resonance.

The characteristic feature of this scenario is the appearance of a small two-component region $\mathcal{R}_2$ within the image $\mathcal{R}$ of EM at small negative x and $|L|$ near 0. In fig. 14, this 3D region is the pyramid-like domain $OCABA'$. Each regular EM value in $\mathcal{R}_2$ lifts to two regular $\mathbb{T}^3$ tori.

As can be seen in fig. 14, the ray $\mathcal{C}_0 = \{\ell_z = h = 0, n > 0\}$ of critical values has three parts. Above point O (where $x = 0$) it is the internal thread of $\mathcal{R}$, below point C it is an edge of the boundary $\partial\mathcal{R}$. Critical values in these parts of $\mathcal{C}_0$ represent the singular fiber $\mathfrak{T}_{x>0}$ and the springing (or stretching for CO_2) 'short' relative equilibrium $\mathbb{S}^1_{\ell_z=0,\, x<x_C}$ respectively. The small part OC of $\mathcal{C}_0$ belongs to the boundary of the two-component region. The inverse image $\mathrm{EM}^{-1}(c)$ of the critical value c in OC consists of two disconnected components; one of which is $\mathbb{S}^1_{\ell_z=0}$ and the other is a regular $\mathbb{T}^3$. Notice that for all $x < 0$, i.e. for all c on $\mathcal{C}_0$ below O, the periodic orbit $\mathbb{S}^1_{\ell_z=0}$ is stable. It becomes hyperbolic unstable in $x = 0$. At the same time the two components of $\mathrm{EM}^{-1}(c)$ for $c \in (OC)$ merge together so that for $x > 0$ the inverse image becomes the curled/pinched 3-torus $\mathfrak{T}_{x>0}$.

In comparison to our discussion in the beginning of sec. 6, we have an additional difficulty due to the higher dimension of $\mathcal{R}$. Unfolding $\mathcal{R}$ requires a fourth dimension. To understand such unfolding, the two component region $\mathcal{R}_2$ should be characterized in more detail. As indicated in fig. 14, $\mathcal{R}_2$ is bounded by the surface $OCABA'$. Only edges AC and $A'C$ of this surface belong to the outer boundary $\partial\mathcal{R}$ of the whole EM image $\mathcal{R}$, the rest of $\overline{\mathcal{R}_2}$ lies inside $\mathcal{R}$. The internal part of the face $AA'O$ consists of points whose inverse image is a singular 3D fiber which can be decomposed as a bitorus times a circle. As we move from this face inside $\mathcal{R}_2$, the inverse image splits into two 3-tori. The $AA'O$ face is therefore a *merger surface* along which the unfolded image $\mathcal{R}$ glues to itself. It is similar to the merger line in fig. 11. The other three faces of $\partial\mathcal{R}_2$ are *degeneracy surfaces*: as we move the value b from inside $\mathcal{R}_2$ and across one of such faces, one of the two regular fibers $\mathbb{T}^3_{b'}$ and $\mathbb{T}^3_{b''}$ which constitute $\mathrm{EM}^{-1}(b)$ degenerates into a 2-torus and then disappears, while the other fiber continues. The important circumstance to notice is that different fibers disappear as we move across different faces: thus if $\mathbb{T}^3_{b'}$ is the one which disappears as we move through the 'bottom' face ACA', then the other fiber $\mathbb{T}^3_{b''}$ disappears as we come out through any of the two 'side' faces ACO or $A'CO$. This proves that the unfolding surface is single sheeted and is a higher dimensional analog of the one shown in fig. 11. Indeed, starting with the value b inside $\mathcal{R}_2$ and taking the component $\mathbb{T}^3_{b''}$ we can deform it continuously (i.e. connect) into $\mathbb{T}^3_{b'}$ as b moves out through one of the side faces, goes deeper into negative energies and down into negative values of x and comes back up to b through the

bottom face. Such connection enables to relate the cycle bases on two components of the same preimage $\mathrm{EM}^{-1}(b)$. Therefore we deal with bidromy.

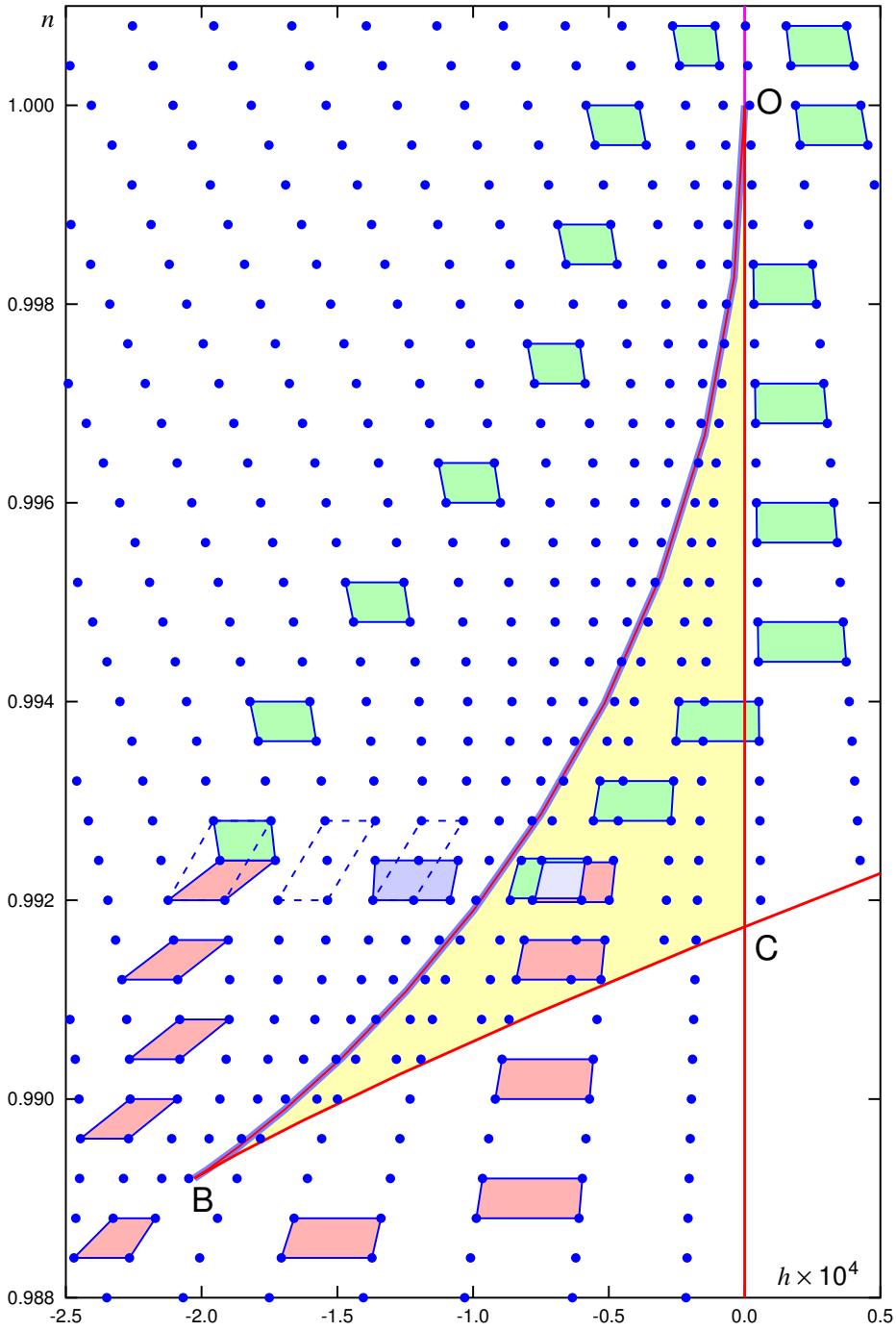

Figure 15. Quantum spectrum (blue dots) of a slightly detuned 1:1:2 resonant oscillator (given by eqs. (5,6) and $y = 1/10$) with $L = 0$ in the (E, x) region corresponding to the existence of two classical fibers. Values of $\hbar = 0.0002$ and $N = 4910 \ldots 5010$ are used in quantum calculations, where $\hbar N = 1 - x$. Elementary cells represent a tentative interpretation of bidromy in terms of cell transportation admitting splitting and fusion of cells at the branching points of the path.

We now describe how such structure of the classical toric fibration manifests itself in the joint energy-momentum eigenvalue spectrum of the corresponding quantum problem. In order to simplify the analysis, we restrict the system to $L = 0$ and consider the respective section of $\mathcal{R}$ in fig. 14 together with the quantum lattice as shown in fig. 15. In this figure, the two component region becomes the 2D domain BCO. Our analysis of the classical system suggests that the joint quantum energy-momentum spectrum

can be unfolded as a regular $\mathbb{Z}^2$ lattice which self-overlaps in the region BCO. Therefore, in this region we should have two sublattices which correspond to two fibers in the inverse images of classical EM values. Indeed these sublattices can be distinguished clearly in fig. 15, and we can also see that one of the sublattices can be continued smoothly out of the self-overlapping region BCO through its right side boundary CO, while the other sublattice continues smoothly through the bottom boundary BC. Far outside BCO the two sublattices join smoothly and become one lattice. It follows that all quantum states represented by the lattice in fig. 15 can be assigned using one system of global quantum numbers. However, states with close energy-momentum and polyad characteristics in the overlap region BCO can have very different quantum numbers if they belong to different sublattices.

The model lattice in fig. 15 stimulates another more sophisticated conjecture on the possibility to transfer a quantum cell across the merger line BO (at which the preimage of the classical EM value splits into a pair of regular tori). We begin with a double cell which splits into two cells after crossing the merger line BO. The new cells belong to two different sublattices. At the same time, the path along which we follow the evolution of the cells splits into two: one goes up around vertex O and the other follows down and turns around B. Each of the two cells is now designated to its own path, and we are obliged to follow their evolution simultaneously. After our cells return back (each along its own path), the resulting cells should be arranged so that they have one common side as shown in fig. 15. Subsequently, we need a procedure to fuse them into a single double cell and to compare the latter to the initial double cell. The transformation between the initial and the final double cell define the quantum *bidromy matrix*. Certainly, in order to justify such construction, the independence of the bidromy transformation on the path should be proven. We intend to develop such formal analysis in a more specialized mathematical paper.

We like to comment that 1:1:2 resonant molecular systems with bidromy are not very likely to exist. Thus all of such systems we know undergo the supercritical bifurcation. In CO_2, where detuning b is ridiculously small, this bifurcation occurs way below the value $n = \frac{3}{2}$ of the ground state; in CS_2 it happens at the level of the first overtone. However, the Fermi resonance and three degrees of freedom are by no means necessary for the system to have bidromy. It is possible to observe this phenomenon in systems with two degrees of freedom [63] and resonance $1:1$ [64].

7 Conclusive remarks

In this paper, we attempted to demonstrate the utility of the concept of monodromy for the qualitative analysis of the dynamics of many fundamental classical Hamiltonian nonlinear dynamical systems and of the energy level structure of the corresponding quantum systems. In the quantum case, monodromy is instrumental for characterization of the patterns in the common eigenvalue spectrum of several commuting operators.

We also liked to show how the study of concrete and even seemingly simple basic systems raises many fundamental questions and suggests formulation of new concepts, such as fractional monodromy or bidromy, which were not known before in formal mathematics. We thus encourage the molecular physics community to intensify its contacts with mathematicians in order to work on the mathematical concepts which can be very helpful in solving many well known physical problems.

On the other hand, we want to point out that understanding physical consequences of formal mathematical characteristics, such as monodromy, require wider participation and initiative. In particular, manifestation of monodromy in the time-domain evolution of quantum systems remains presently an almost completely open question.

References

[1] J.J. Duistermaat, *Comm. Pure Appl. Math.*, **33**, 687 (1980).
[2] N. N. Nekhoroshev, *Trans. Moscow Math. Soc.*, **26**, 180 (1972).
[3] R. H. Cushman and J. J. Duistermaat, *Bull. Am. Math. Soc.*, **19**, 475 (1988).
[4] R. H. Cushman, *Centrum voor Wiskunde en Informatica Newsletter*, **1**, 4 (1983).
[5] L. M. Bates and R. H. Cushman, *Global aspects of classical integrable systems* (Birkhäuser, Basel, 1997).
[6] R. H. Cushman and D. A. Sadovskiĭ, *Europhys. Lett*, **47**, 1 (1999).
[7] R. H. Cushman and D. A. Sadovskiĭ, *Physica D*, **142**, 166 (2000).

[8] K. Efstathiou, R. H. Cushman, and D. A. Sadovskiĭ, *Physica D*, **194**, 250 (2004).
[9] D. A. Sadovskiĭ and B. I. Zhilinskiĭ, *Phys. Lett. A*, **256**, 235 (1999).
[10] L. Grondin, D. A. Sadovskiĭ, and B. I. Zhilinskiĭ, *Phys. Rev. A*, **142**, 012105 (2002).
[11] M. S. Child, T. Weston, and J. Tennyson, *Mol. Phys.*, **96**, 371 (1999).
[12] N. F. Zobov, S. V. Shirin, O. L. Polyansky, J. Tennyson, P.-F. Coheur, P. F. Bernath, M. Carleer, R. Colin, *Chem. Phys. Lett.*, **414**, 193 (2005).
[13] H. Waalkens, A. Junge, and H. R. Dullin, *J. Phys. A. Math. Gen.*, **36**, L307 (2003).
[14] H. Waalkens, H. R. Dullin, and P. H. Richter, *Physica D*, **196**, 265 (2004).
[15] M. Joyeux, D. A. Sadovskiĭ, and J. Tennyson, *Chem. Phys. Lett.*, **382**, 439 (2003).
[16] K. Efstathiou, M. Joyeux, and D. A. Sadovskiĭ, *Phys. Rev. A*, **69**, 032504 (2004).
[17] R. H. Cushman, H. R. Dullin, A. Giacobbe, D. D. Holm, M. Joyeux, P. Lynch, D. A. Sadovskiĭ, B. I. Zhilinskiĭ, *Phys. Rev. Lett.*, **93**, 024302 (2004).
[18] A. Giacobbe, R. H. Cushman, D. A. Sadovskiĭ, and B. I. Zhilinskiĭ, *J. Math. Phys.*, **45**, 5076 (2004).
[19] C. D. Cooper and M.S. Child, Phys. Chem. Chem. Phys. **7**, 2731 (2005); note that Figures 7 and 8 of this paper are corrected in [27].
[20] I. N. Kozin and R. M. Roberts, *J. Chem. Phys.*, **118**, 10523 (2003).
[21] C. A. Arango, W. W. Kennerly, and G. S. Ezra, *Chem. Phys. Lett.*, **392**, 486 (2004); *J. Chem. Phys.*, **122**, 184303 (2005)
[22] K. Efstathiou, *Metamorphoses of Hamiltonian Systems with Symmetry*, Lect. Notes in Math. **1864** (Springer-Verlag, Heidelberg, 2004).
[23] S. Vũ Ngọc,*Comm. Math. Phys.*, **203**, 465 (1999).
[24] N. N. Nekhoroshev, D. A. Sadovskiĭ, and B. I. Zhilinskiĭ, *Annales Henri Poincaré*, accepted for publication (2006).
[25] B. I. Zhilinskiĭ, *Acta Appl. Math.*, **87**, 281 (2005).
[26] B. I. Zhilinskii, in: *Topology in Condensed matter*, Ed. M. Monastyrsky (Springer Series in Solid State Sciences, vol. 150, 2006), p. 165.
[27] M. Child, *Adv. Chem. Phys.* (in press).
[28] M. Audin, *Topology of torus actions on symplectic manifolds* (Birkhäusser, Boston, 1991).
[29] V. Guillemin, *Moment Maps and Combinatorial Invariants of Hamiltonian T^n-spaces* (Birkhäuser, Boston, 1994).
[30] J.-M. Souriau, *Structure of Dynamical Systems: a symplectic view of physics*, English translation by C. H. Cushman–de Vries, Editors R. H. Cushman and G. M. Tuynman, Birkhäuser, Boston, 1997. Original French edition: *Structure des systèmes dynamiques*, Dunod, Paris, 1970.
[31] Vl.I. Arnol'd, *Mathematical Methods of Classical Mechanics*, vol. 60 of *Graduated Texts in Mathematics*, 2nd edition, Translated by K. Vogtmann and A. Weinstein, Springer-Verlag, New York, 1989.
[32] H. Broer, R. H. Cushman, F. Fassò, F. Takens, *Geometry of KAM-tori for nearly integrable Hamiltonian systems*, preprint, University of Gröningen, 2002; `arXiv:math.DS/0210043`.
[33] B. Rink, *Nonlinearity*, **17**, 347 (2004).
[34] M. C. Gutzwiller, *Chaos in classical and quantum mechanics*, Ser. Interdisciplinary applied mathematics, Vol. 1, Springer, New York, 1990; chapt. 14.
[35] V. S. Matveev, Sb. Math. **187**, No.4 (1996) 495–524.
[36] L. M. Lerman and Ya. L. Umanskiĭ, *Four dimensional integrable Hamiltonian systems with simple singular points*, Transl. Math. Monographs **176**, American Math. Soc., Providence, R.I., 1998.
[37] R. H. Cushman and J. J. Duistermaat, *J. Diff. Eq.*, **172**, 42 (2001).
[38] N. T. Zung, Diff. Geom. Appl. **7** (1997) 123–130; Lett. Math. Phys. **60** (2002) 87–99.
[39] A. V. Bolsinov and A. T. Fomenko, *Integrable Hamiltonian systems. Geometry, topology, classification*, Chapman & Hall/CRC, 2004.
[40] N. N. Nekhoroshev, D. A. Sadovskiĭ, and B. I. Zhilinskiĭ, *C. R. Acad. Sci. Paris*, Ser. I, **335**, 985 (2002).
[41] K. Efstathiou, R. H. Cushman, and D. A. Sadovskiĭ, *Adv. Math.*, accepted for publication (2006).
[42] Y. Colin de Verdier and S. Vũ Ngọc, *Ann. Ec. Norm. Sup.*, **36**, 1 (2003).
[43] N. Fulton, J. Tennyson, D. A. Sadovskiĭ, and B. I. Zhilinskiĭ, *J. Chem. Phys.*, **99**, 906 (1993).
[44] I. N. Kozin, D. A. Sadovskiĭ, and B. I. Zhilinskiĭ, *Spectrochim. Acta A*, **61**(13-14) 2867 (2005).
[45] K. Efstathiou and D. A. Sadovskiĭ, *Nonlinearity*, **17**, 415 (2004).
[46] K. Efstathiou, R. H. Cushman, and D. A. Sadovskiĭ, *Proc. Roy. Soc. Lond. Ser. A* **459**, 2997 (2003).
[47] K. Efstathiou, D. A. Sadovskiĭ, and B. I. Zhilinskiĭ, *SIADS (SIAM Journal of Applied Dynamical Systems)*, **3**(3), 261 (2004).
[48] L. M. Bates. Proc. Roy. Soc. Edinbourg, **110**A, 27 (1988).
[49] M. Gross, Special Lagrangian Fibrations. I. Topology, in: *Integrable Systems and Algebraic Geometry*, Ed. by M.-H. Saito, Y. Shimuzu, and K. Ueno, World Scientific 1998, 156–193.
[50] M. Gross, Special Lagrangian Fibrations. II: Geometry, in: *Surveys in Differential Geometry*, Somerville, MA, International Press 1999, 341–403.
[51] M. Gross, *Invent. math.*, **144**, 75 (2001).
[52] L. R. Bates, J. Appl. Math. Phys. (ZAMP), **42**, 837 (1991).
[53] M. Child, *J. Phys. A: Math. Gen.*, **31**, 657 (1998).
[54] R. N. Dixon, *Trans. Faraday Soc.*, **60**, 1363 (1964).
[55] D. D. Holm and P. Lynch, SIAM J. Appl. Dyn. Syst. **1**, 44 (2002).
[56] P. Lynch, Int. J. Nonlin. Mech. **37**, 345 (2002).
[57] H. Dullin, A. Giacobbe, and R. H. Cushman, Physica D **190**, 15 (2004).
[58] L. Xiao and M. E. Kellman, J. Chem. Phys. **93**, 5805 (1990).
[59] C. Zhou, D. Xie, R. Chen, G. Yan, H. Guo, V. Tyng, M. Kellman, Spectrochim. Acta A, **58**, 727 (2002).
[60] M. Joyeux, S. C. Farantos, and R. Schinke, *J. Phys. Chem. A*, **106**, 5407 (2002).
[61] *No Polar Coordinates. Lectures by Richard Cushman*, prepared by K. Efstathiou and D. A. Sadovskiĭ, in *Geometric Mechanics and Symmetry. The Peyresq Lectures*, Editors James Montaldi and Tudor Ratiu, London Mathematical Society Lecture Note Series No. 306 (Cambridge University Press, Cambridge, UK, 2005)
[62] J. C. van der Meer, *The Hamiltonian Hopf bifurcation*, Vol. 1160, Lect. Notes in Math. Springer, New York, 1985.
[63] D. Sugny, M. Joyeux, and H. R. Jauslin, private communication.
[64] A. Giacobbe, private communication.